

SUPA, School of Physics and Astronomy
Experimental Particle Physics Group
Kelvin Building, University of Glasgow,
Glasgow, G12 8QQ, Scotland
Telephone: +44 (0)141 330 2000 Fax: +44 (0)141 330 5881

NLO QCD corrections to tW' and tZ' production in forward-backward asymmetry models

J. Adelman¹, J. Ferrando², C. D. White²

¹ Department of Physics, Yale University, New Haven CT, USA

² SUPA, School of Physics and Astronomy, University of Glasgow, Glasgow, G12 8QQ, Scotland

Abstract

We consider Z' and W' models recently proposed to explain the top forward-backward asymmetry at the Tevatron. We present the next-to-leading order QCD corrections to associated production of such vector bosons together with top quarks at the Large Hadron Collider, for centre-of-mass energies of 7 and 8 TeV. The corrections are significant, modifying the total production cross-section by 30-50%. We consider the effects of the corrections on the top and vector-boson kinematics. The results are directly applicable to current experimental searches, for both the ATLAS and CMS collaborations.

1 Introduction

Top-quark physics remains a highly active research area, both theoretically and experimentally. The close proximity of the top-quark mass to the electroweak symmetry breaking scale, and the possible role of new physics in explaining this symmetry breaking, mean that the top-quark sector may provide a clear window through which to look for beyond the Standard Model effects. Furthermore, the Large Hadron Collider offers top-quark production rates far in excess of previous colliders, allowing detailed scrutiny of the top quark and its interactions. A complementary view is provided by the Tevatron which, despite having a lower centre of mass energy, has an antisymmetric ($p\bar{p}$) initial state, which can probe different aspects of top-quark behaviour to the LHC. One such feature is the forward-backward asymmetry of $t\bar{t}$ pairs, which has been measured to be in excess of the Standard Model prediction [1–7] by both D0 and CDF [8–10], and which has generated much subsequent theoretical interest.

In this paper we focus on a particular new physics scenario motivated by the forward-backward asymmetry, namely the existence of W' and (flavour-changing) Z' bosons. These have been considered in a number of recent studies (see e.g. [11–38]). In some of these works (e.g. [14]), the new gauge bosons emerge from a complete beyond the Standard Model theory with extended gauge group. In other more phenomenological studies, the fundamental origin of the new gauge bosons is not spelled out explicitly. This is sufficient for the study of particular scattering processes, in that the interaction Lagrangian for a W' or Z' boson with Standard Model quarks can be written in a generic form which is independent of the underlying theory. Note also that coupling and parameter definitions (including overall normalisations) differ in the above literature. Here we will focus our discussion explicitly on the model of [29].

Although motivated by the sizeable forward-backward asymmetry, W' and Z' models must face a number of stringent experimental constraints, including precision electroweak observables [39]; the neutron electric dipole moment [40, 41]; same-sign top production [42, 43]; the top-quark pair production cross-section at the Tevatron [44, 45] and LHC [46, 47]; and the top-quark charge asymmetry at the LHC [48, 49]. As recent analyses have pointed out [31, 32, 50], there is already tension between existing constraints and theoretical predictions, such that significant fractions of parameter space in such models are already being ruled out. In particular, there seems to be some incompatibility between the measured LHC charge asymmetry, and the Tevatron forward-backward asymmetry, if both are to have a common origin in terms of W' - and Z' -boson exchange.

Given the above experimental constraints on W' and Z' models, it is also important, experimentally, to explore every possible production mechanism involving W' and Z' bosons, so that cross-checks can be made of the conclusions reached from different observables. A crucial process in this regard is the direct production of such a gauge boson in association with a single top quark, and indeed this process is being actively sought by the ATLAS, CDF [51] and CMS [52] collaborations ¹⁾. These searches result in direct bounds on the masses of the new gauge bosons, and on their couplings to the quarks. These are upper and lower bounds for the couplings and masses respectively, and in order for these to be as tight as possible, it is preferable to include higher order perturbative

¹⁾Analyses may differ in whether they choose to focus explicitly on the kinematic region of resonant gauge boson production, as we discuss further in section 5.

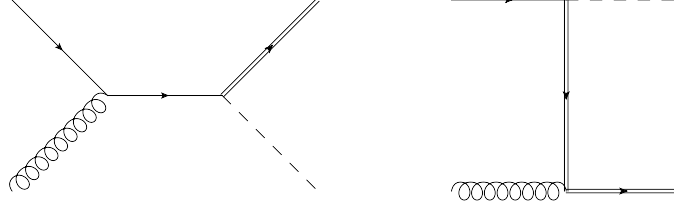


Figure 1: Leading order diagrams for associated production of a W' or Z' (dashed line) with a top quark (double line). The single fermion line represents an appropriate down or up-type quark.

corrections to the relevant cross-sections.

The aim of this paper is to present the complete NLO QCD corrections to the production of a W' or Z' boson in association with a top (or anti-top) quark, for both total cross sections and kinematic distributions of the top quark and new gauge bosons. Our results can be used directly in relevant experimental analyses, where they can be used to strengthen the bounds on the parameter space of models involving these bosons. Our intention is to be as model-independent as possible, so that our results can be combined to yield total cross sections for various scenarios. We will see that NLO corrections are significant for total rates (potentially of the order of 50% for central values, and rising with the mass of the gauge boson), which by itself justifies the calculation of higher-order corrections, due to the potentially significant impact on extracted bounds on parameter space.

The structure of the paper is as follows. In section 2, we describe technical details relating to our NLO calculation, noting similarities to Standard Model Wt production, which was first considered in [53], and calculated at NLO in [54, 55]. In section 3 we present results for total cross sections, examining also kinematic distributions in section 4. In section 5 we consider the implications of our results for current LHC searches. In section 6, we discuss our results before concluding. Various additional results are collected in the supplementary material accompanying this submission, which can be found in Appendix A of this preprint version.

2 Calculation of NLO corrections

In this section, we describe the technical details of our NLO calculation. Note that many of these details are very similar to the (Standard Model) Wt calculation presented in [56], thus we will be brief. Unless otherwise stated, we will explicitly refer to top-quark production as opposed to antitop-quark production. Similar remarks apply in the latter case.

We consider NLO QCD corrections to the process

$$q(p_1) + g(p_2) \rightarrow t(k_1) + X^-(k_2), \quad (1)$$

where q is an appropriate quark, and X is either a W' or Z' boson. The LO diagrams are shown in figure 1. Following [29], we define the coupling of these bosons to the top quark according to the

Lagrangians

$$\begin{aligned}\mathcal{L}_{W'} &= \frac{P_{tD}}{\sqrt{2}} \bar{D} \gamma^\mu g_R P_R t W' + \text{h.c.}; \\ \mathcal{L}_{Z'} &= \frac{Q_{tU}}{\sqrt{2}} \bar{U} \gamma^\mu g_R P_R t Z' + \text{h.c.},\end{aligned}\tag{2}$$

where g_R is a coupling constant, P_R the right-handed projection operator, and U , D denote generic up-type and down-type quarks. The model of [29] considers only couplings between the first and third quark generations. In order to increase the flexibility of our calculation, we here generalise this by including also couplings between the top quark and arbitrary up and down-type quarks. The additional coupling factors P_{tD} and Q_{tU} play a role analogous to CKM matrix elements. Note that we carry out our calculation in a five-flavour parton scheme, so that initial states involving b quarks are also included in the total $W't$ cross section.

Note that the Lagrangian of eq. (4) is specific in the sense that the coupling involves the pure right-handed projection operator P_R . In principle, there could be a mixture of left- and right-handed projectors, with corresponding couplings g_R and g_L . However, analogously to Standard Model Wt production up to NLO [54,55], the total cross section is proportional to the combination $|g_L|^2 + |g_R|^2$. Hence, total cross sections and kinematic distributions of the top and gauge bosons can be simply rescaled in the presence of both left- and right-handed couplings. Note, however, that the relative mixture of these would be important in considering distributions relating to the decay products of the top quark and gauge boson.

As in [56,57], we use the on-shell scheme for renormalisation of the top-quark mass and QCD coupling [58] (this modifies the $\overline{\text{MS}}$ -scheme renormalisation of the latter, such that the top-quark loop contribution is subtracted on-shell). The Feynman diagrams for the virtual corrections are exactly the same as those for Standard Model Wt production [54,55], although all finite parts of scalar integrals must be analytically continued to the kinematic region $m_X > m_t$. We use the results of [59], as implemented in a previous H^-t calculation involving one of the authors [57].

For the real emission corrections, all Feynman diagrams have the same form as Standard Model Wt production, for which we use results from a previous calculation involving one of the present authors [56]. In the latter case, however, an on-shell subtraction scheme is necessary in order to define the scattering process at NLO i.e. by removing the contribution from leading order top pair production [56,60–64]. Here no such difficulties arise, due to the fact that we explicitly consider the regime $m_X > m_t$. Further differences with Wt production arise in that the partonic channels are different in the present case. One must also replace the electroweak coupling and CKM matrix with the relevant coupling factors from eq. (4).

In order to be able to numerically compute cross sections in a stable manner, the real and virtual corrections must be regularised and combined using an appropriate subtraction formalism for soft and collinear singularities, of which a number exist in the literature [65–69]. Here, as in [56], we use the FKS formalism of [65].

3 Total cross section for tW' and tZ' production

In this section, we present results for total NLO cross sections, for the process of eq. (1). For ease of comparison with e.g. [29], we begin by considering the Lagrangian of eq. (4) with a non-zero coupling between the first and third generations only. That is, $P_{td} = Q_{tu} = 1$ and $P_{ts} = P_{tb} = Q_{tc} = 0$. Furthermore, we fix $g_R = 1$, and use default renormalisation and factorisation scale choices of $\mu_R = \mu_F = (m_t + m_X)/2$, where m_X is the mass of the W' or Z' boson, as appropriate, and $m_t = 172.5$ GeV is the top quark mass. We consider the LHC, with a centre of mass energy of 7 TeV.

Results for the total cross section (i.e. the sum of both top and antitop production) at LO and NLO are shown for both Z' and W' production in tables 1–4. We show all results using both CTEQ [70, 71]²⁾ and MSTW [72] partons, where appropriate we calculate the parton distribution function (PDF) uncertainty using the relevant PDF error sets. In all subsequent plots, we show results using MSTW partons unless otherwise stated. For each result, we also present the scale variation uncertainty obtained by varying both μ_F and μ_R independently in the range $\mu_0/2, 2\mu_0$, where μ_0 is the default scale. One sees that the scale variation uncertainty is reduced at NLO, as expected. Furthermore, the PDF uncertainty with MSTW partons is much smaller than the scale uncertainty. This is also to be expected, given that the cross section is dominated by the production of top quarks involving a u or d quark in the initial state (for Z' and W' production respectively), namely valence quarks. Furthermore, the heavy nature of the final state (involving both a top quark and a heavy vector boson) means that the partons are evaluated at typically high momentum fractions x . Valence quark distributions at high x are well constrained by global PDF fits, hence the small PDF uncertainty in the results of tables 1-4. With CTEQ partons the PDF uncertainty is of a similar size to the scale uncertainty over most of the mass range, becoming larger than the scale uncertainty at very high mass. This larger PDF uncertainty is partly due to the fact that the CTEQ uncertainties represent 90% confidence intervals whereas the MSTW uncertainties represent 68% confidence intervals³⁾. Plots of the total cross sections for Z' and W' production are shown in figures 2 and 3, where we have added the PDF and scale uncertainties in quadrature.

In figures 4 and 5, we show the K -factor for both Z' and W' production as a function of the mass of the gauge boson m_X , evaluated according to

$$K = \frac{\sigma_{\text{NLO}}}{\sigma_{\text{LO}}}, \quad (3)$$

where we have used the results obtained with MSTW partons from tables 1-4. We see that the K -factor is sizeable and increasing with m_X . For the values of m_X we consider, the NLO corrections range from $\simeq 30\% - 50\%$ in both cases. This can be compared with Standard Model Wt production, for which the K -factor is $\simeq 25\%$ [54, 55], subject to an appropriate on-shell subtraction formalism being employed to separate the Wt mode from top pair production. The higher K factor in the present case, and the fact that the K -factor rises with increasing gauge boson mass, have partonic origins. As stated above, both W' and Z' production have valence quarks in the initial state. Furthermore, as m_X increases, these distributions are probed at typically higher x values, and relatively more so at NLO. Given that valence quark distributions remain significant at higher

²⁾For ease of comparison with existing literature, we provide results with CTEQ6L1 partons at LO.

³⁾This is typically accounted for by dividing the CTEQ uncertainties by a factor 1.645 [73].

| $M(Z') \text{ (GeV)}$ | $\sigma_{\text{born}}^{\text{CTEQ6L1}}(tZ' + \bar{t}Z') \text{ (pb)}$ | $\sigma_{\text{born}}^{\text{MSTW 2008 LO}}(tZ' + \bar{t}Z') \text{ (pb)}$ |
|-----------------------|---|--|
| 200 | 77.9 +16.3 -12.5 | 79.3 +17.4 -13.2 |
| 300 | 26.65 +5.93 -4.50 | 27.28 +6.37 -4.79 |
| 400 | 10.81 +2.52 -1.90 | 11.15 +2.74 -2.04 |
| 500 | 4.89 +1.18 -0.88 | 5.08 +1.30 -0.96 |
| 600 | 2.39 +0.60 -0.44 | 2.50 +0.66 -0.49 |
| 700 | 1.234 +0.316 -0.233 | 1.306 +0.358 -0.260 |
| 800 | 0.667 +0.175 -0.128 | 0.713 +0.201 -0.145 |
| 900 | 0.373 +0.100 -0.073 | 0.402 +0.117 -0.084 |
| 1000 | 0.215 +0.059 -0.043 | 0.234 +0.069 -0.050 |
| 1100 | 0.126 +0.035 -0.025 | 0.139 +0.042 -0.030 |
| 1200 | 0.0759 +0.0214 -0.0155 | 0.0840 +0.0261 -0.0185 |
| 1300 | 0.0463 +0.0133 -0.0096 | 0.0516 +0.0164 -0.0115 |
| 1400 | 0.0286 +0.0083 -0.0060 | 0.0321 +0.0104 -0.0073 |
| 1500 | 0.0178 +0.0053 -0.0038 | 0.0202 +0.0067 -0.0047 |
| 1600 | 0.0112 +0.0034 -0.0024 | 0.0128 +0.0043 -0.0030 |
| 1700 | 0.0071 +0.0022 -0.0015 | 0.0082 +0.0028 -0.0019 |
| 1800 | 0.00455 +0.00139 -0.00099 | 0.00527 +0.00184 -0.00126 |
| 1900 | 0.00292 +0.00090 -0.00064 | 0.00340 +0.00121 -0.00083 |
| 2000 | 0.00188 +0.00059 -0.00042 | 0.00220 +0.00080 -0.00054 |

Table 1: The sum of the leading-order cross sections for $pp \rightarrow tZ'$ and $pp \rightarrow \bar{t}Z'$ at the 7 TeV LHC. Scale and PDF uncertainties are given first and second respectively. In the case of the CTEQ6L1 PDFs no PDF uncertainty exists.

| $M(W')$ (GeV) | $\sigma_{\text{born}}^{\text{CTEQ6L1}}(tW'^- + \bar{t}W'^+) \text{ (pb)}$ | $\sigma_{\text{born}}^{\text{MSTW 2008 LO}}(tW'^- + \bar{t}W'^+) \text{ (pb)}$ |
|---------------|---|--|
| 200 | 41.8 +9.1 -7.0 +3.15 | 42.7 +9.8 -7.4 +3.42 |
| 300 | 13.60 -2.37 +1.28 | 13.92 -2.54 +1.40 |
| 400 | 5.26 -0.95 +0.57 | 5.41 -1.03 +0.63 |
| 500 | 2.28 -0.42 +0.277 | 2.35 -0.46 +0.309 |
| 600 | 1.068 -0.203 +0.141 | 1.109 -0.223 +0.159 |
| 700 | 0.531 -0.103 +0.075 | 0.554 -0.114 +0.086 |
| 800 | 0.276 -0.055 +0.041 | 0.290 -0.061 +0.048 |
| 900 | 0.149 -0.030 +0.0234 | 0.157 -0.034 +0.0273 |
| 1000 | 0.0829 -0.0169 +0.0135 | 0.0879 -0.0193 +0.0160 |
| 1100 | 0.0472 -0.0098 +0.0080 | 0.0502 -0.0112 +0.0095 |
| 1200 | 0.0274 -0.0057 +0.0048 | 0.0293 -0.0067 +0.0058 |
| 1300 | 0.0161 -0.0034 +0.0029 | 0.0173 -0.0040 +0.0035 |
| 1400 | 0.0097 -0.0021 +0.0018 | 0.0104 -0.0024 +0.0022 |
| 1500 | 0.0058 -0.0013 +0.00109 | 0.0063 -0.0015 +0.00136 |
| 1600 | 0.00356 -0.00078 +0.00068 | 0.00386 -0.00093 +0.00085 |
| 1700 | 0.00218 -0.00048 +0.00042 | 0.00238 -0.00058 +0.00054 |
| 1800 | 0.00135 -0.00030 +0.00027 | 0.00147 -0.00036 +0.00034 |
| 1900 | 0.00084 -0.00019 +0.00017 | 0.00092 -0.00023 +0.00022 |
| 2000 | 0.00052 -0.00012 | 0.00057 -0.00015 |

Table 2: The sum of the leading-order cross sections for $pp \rightarrow tW'^-$ and $pp \rightarrow \bar{t}W'^+$ at the 7 TeV LHC. Other details as in table 1.

| $M(Z')$ (GeV) | $\sigma_{\text{nlo}}^{\text{CT10}}(tZ' + \bar{t}Z')$ (pb) | | | $\sigma_{\text{nlo}}^{\text{MSTW 2008 NLO}}(tZ' + \bar{t}Z')$ (pb) | | |
|---------------|---|----------------------|----------------------|--|----------------------|----------------------|
| 200 | 101.2 | +6.7 -7.1 | +2.1 -3.1 | 103.6 | +7.0 -7.5 | +0.7 -1.1 |
| 300 | 35.32 | +2.29 -2.59 | +0.93 -1.26 | 36.10 | +2.42 -2.71 | +0.26 -0.41 |
| 400 | 14.61 | +0.96 -1.12 | +0.50 -0.60 | 14.92 | +1.01 -1.17 | +0.13 -0.20 |
| 500 | 6.74 | +0.46 -0.54 | +0.30 -0.32 | 6.87 | +0.48 -0.56 | +0.08 -0.10 |
| 600 | 3.35 | +0.23 -0.28 | +0.18 -0.19 | 3.41 | +0.25 -0.29 | +0.05 -0.06 |
| 700 | 1.769 | +0.128 -0.153 | +0.115 -0.114 | 1.795 | +0.134 -0.158 | +0.033 -0.038 |
| 800 | 0.975 | +0.073 -0.087 | +0.075 -0.072 | 0.987 | +0.077 -0.090 | +0.022 -0.024 |
| 900 | 0.557 | +0.044 -0.051 | +0.050 -0.046 | 0.561 | +0.045 -0.053 | +0.015 -0.016 |
| 1000 | 0.327 | +0.027 -0.031 | +0.034 -0.030 | 0.328 | +0.028 -0.032 | +0.010 -0.011 |
| 1100 | 0.197 | +0.017 -0.019 | +0.023 -0.020 | 0.196 | +0.017 -0.020 | +0.007 -0.007 |
| 1200 | 0.121 | +0.011 -0.012 | +0.017 -0.014 | 0.120 | +0.011 -0.012 | +0.005 -0.005 |
| 1300 | 0.0752 | +0.0068 -0.0078 | +0.0117 -0.0093 | 0.0740 | +0.0069 -0.0079 | +0.0032 -0.0033 |
| 1400 | 0.0475 | +0.0045 -0.0051 | +0.0084 -0.0063 | 0.0463 | +0.0045 -0.0051 | +0.0023 -0.0022 |
| 1500 | 0.0303 | +0.0030 -0.0034 | +0.0060 -0.0044 | 0.0293 | +0.0030 -0.0033 | +0.0016 -0.0015 |
| 1600 | 0.0195 | +0.0020 -0.0022 | +0.0044 -0.0031 | 0.0187 | +0.0020 -0.0022 | +0.0011 -0.0011 |
| 1700 | 0.0127 | +0.0013 -0.0015 | +0.0032 -0.0022 | 0.0120 | +0.0013 -0.0014 | +0.0008 -0.0008 |
| 1800 | 0.0083 | +0.0009 -0.0010 | +0.0023 -0.0015 | 0.0078 | +0.0009 -0.0010 | +0.0005 -0.0005 |
| 1900 | 0.0055 | +0.0006 -0.0007 | +0.0017 -0.0011 | 0.0050 | +0.0006 -0.0006 | +0.0004 -0.0004 |
| 2000 | 0.00360 | +0.00042 -0.00046 | +0.00127 -0.00078 | 0.00328 | +0.00039 -0.00042 | +0.00025 -0.00025 |

Table 3: The sum of the next-to-leading-order cross sections for $pp \rightarrow tZ'$ and $pp \rightarrow \bar{t}Z'$ at the 7 TeV LHC. Scale and PDF uncertainties are given first and second respectively.

| $M(W')$ (GeV) | $\sigma_{\text{nlo}}^{\text{CT10}}(tW'^- + \bar{t}W'^+) \text{ (pb)}$ | | | $\sigma_{\text{nlo}}^{\text{MSTW 2008 NLO}}(tW'^- + \bar{t}W'^+) \text{ (pb)}$ | | |
|---------------|---|----------------------|----------------------|--|----------------------|----------------------|
| 200 | 55.6 | +3.7 -4.0 | +2.1 -2.7 | 57.1 | +3.9 -4.3 | +0.5 -0.9 |
| 300 | 18.48 | +1.22 -1.40 | +0.83 -1.00 | 18.83 | +1.29 -1.47 | +0.21 -0.34 |
| 400 | 7.32 | +0.49 -0.58 | +0.40 -0.45 | 7.40 | +0.52 -0.61 | +0.10 -0.16 |
| 500 | 3.24 | +0.23 -0.27 | +0.22 -0.23 | 3.25 | +0.24 -0.28 | +0.06 -0.08 |
| 600 | 1.555 | +0.112 -0.134 | +0.122 -0.123 | 1.546 | +0.117 -0.137 | +0.033 -0.045 |
| 700 | 0.792 | +0.060 -0.071 | +0.073 -0.070 | 0.780 | +0.061 -0.072 | +0.020 -0.026 |
| 800 | 0.423 | +0.033 -0.039 | +0.046 -0.042 | 0.411 | +0.034 -0.039 | +0.013 -0.015 |
| 900 | 0.234 | +0.019 -0.022 | +0.029 -0.026 | 0.225 | +0.019 -0.022 | +0.008 -0.009 |
| 1000 | 0.134 | +0.011 -0.013 | +0.019 -0.016 | 0.127 | +0.011 -0.013 | +0.005 -0.006 |
| 1100 | 0.0781 | +0.0069 -0.0080 | +0.0127 -0.0103 | 0.0729 | +0.0068 -0.0077 | +0.0034 -0.0037 |
| 1200 | 0.0466 | +0.0043 -0.0049 | +0.0086 -0.0067 | 0.0428 | +0.0041 -0.0047 | +0.0022 -0.0024 |
| 1300 | 0.0283 | +0.0027 -0.0031 | +0.0059 -0.0044 | 0.0255 | +0.0026 -0.0029 | +0.0015 -0.0016 |
| 1400 | 0.0174 | +0.0017 -0.0019 | +0.0041 -0.0030 | 0.0154 | +0.0016 -0.0018 | +0.0010 -0.0010 |
| 1500 | 0.0108 | +0.0011 -0.0012 | +0.0029 -0.0020 | 0.0094 | +0.0010 -0.0011 | +0.0007 -0.0007 |
| 1600 | 0.0068 | +0.0007 -0.0008 | +0.0020 -0.0014 | 0.0058 | +0.0007 -0.0007 | +0.0004 -0.0005 |
| 1700 | 0.00434 | +0.00048 -0.00053 | +0.00143 -0.00094 | 0.00358 | +0.00042 -0.00045 | +0.00030 -0.00030 |
| 1800 | 0.00277 | +0.00032 -0.00035 | +0.00102 -0.00065 | 0.00223 | +0.00027 -0.00029 | +0.00020 -0.00020 |
| 1900 | 0.00178 | +0.00021 -0.00023 | +0.00073 -0.00045 | 0.00139 | +0.00017 -0.00018 | +0.00013 -0.00013 |
| 2000 | 0.00115 | +0.00014 -0.00015 | +0.00052 -0.00031 | 0.00087 | +0.00011 -0.00012 | +0.00009 -0.00009 |

Table 4: The sum of the next-to-leading-order cross sections for $pp \rightarrow tW'^-$ and $pp \rightarrow \bar{t}W'^+$ at the 7 TeV LHC. Other details as in table 3.

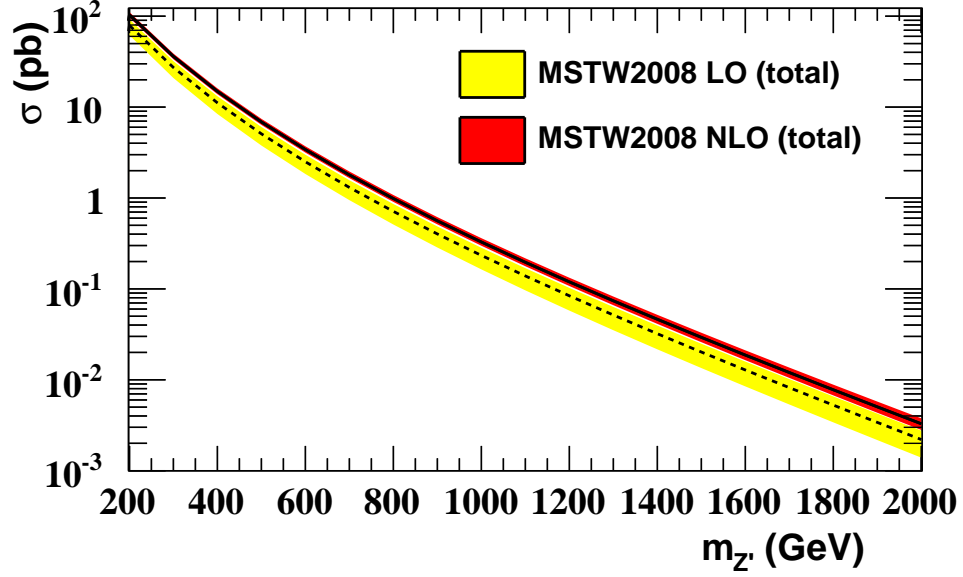


Figure 2: The total cross section for Z' production at LO (dashed) and NLO (solid), together with combined scale and PDF uncertainties.

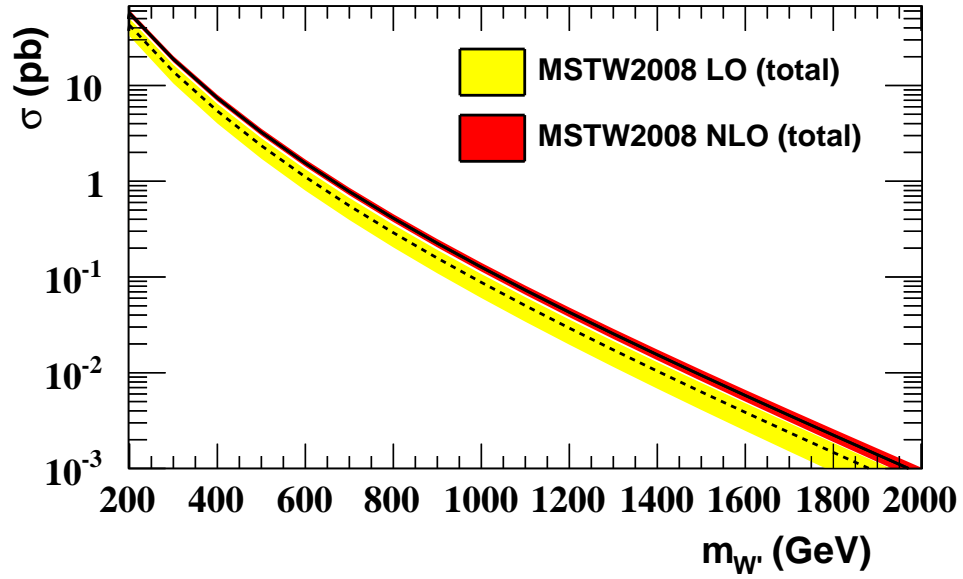


Figure 3: The total cross section for W' production at LO (dashed) and NLO (solid), together with combined scale and PDF uncertainties.

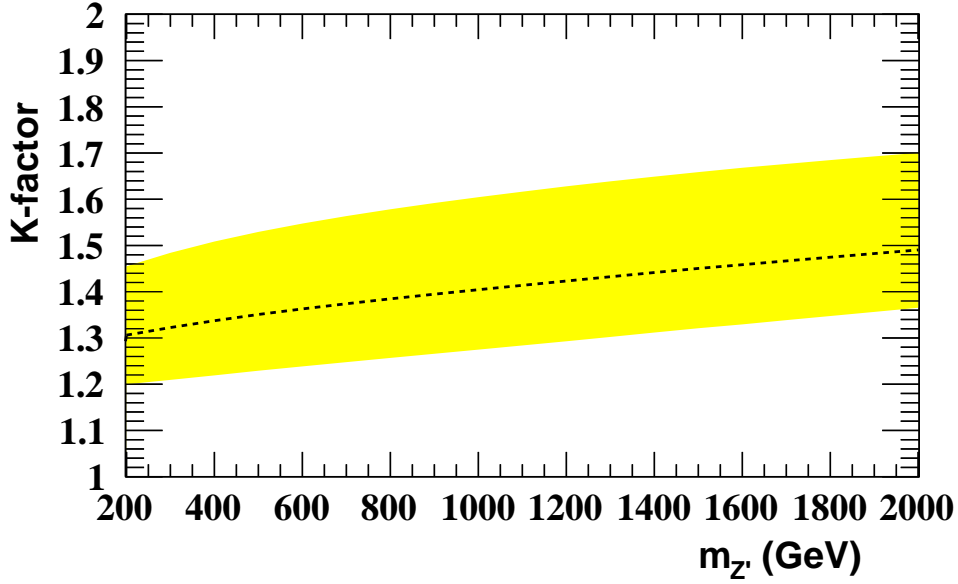


Figure 4: The K -factor for Z' production as defined in eq. (3), with combined scale and PDF uncertainty.

x values, the K -factor is therefore sizable. One may find the opposite trend if sea or b quarks are involved in the initial state i.e. a K -factor which decreases with increasing m_X , due to the sharp fall-off in the partons as $x \rightarrow 1$ (we consider other partonic couplings in the supplementary document). Note that there are also extra partonic subchannels which open up at NLO (i.e. the $q\bar{q}$ and gg initial states), which also act to increase the K -factor.

From tables 1–4 and figures 4–5, one sees that the K -factor for W' production is slightly larger than that for Z' production. This can be explained by the fact that the former case has d quarks in the initial state rather than u quarks. The heavy final state means that these partons are typically probed at high x values, where the u quark distribution (at LO or NLO) has a pronounced shoulder (followed by a steep fall off) relative to the d quark distribution [72]. At NLO, the partons are probed at higher x values than at LO, which leads to a decrease in the parton luminosity. This is less marked for the d distribution than for the u distribution, due to the shoulder in the latter. Hence, the K -factor for W' production is slightly larger than that for Z' production ⁴⁾.

As well as the total cross section, it is also interesting to consider the fraction of events containing a top quark, rather than an anti-top quark (in the case of W' production, this changes the sign of the charge of the accompanying boson). This fraction is shown for Z' and W' production in

⁴⁾Another reason for the K -factor difference is due to additional partonic subchannels opening up at NLO, with gg and $q\bar{q}$ initial states, which contribute different fractions of the total cross-sections in $W't$ and $Z't$ production. However, this has a small effect on the K -factor difference, due to the fact that the NLO cross-section remains dominated by $q\bar{q}$ initial states.

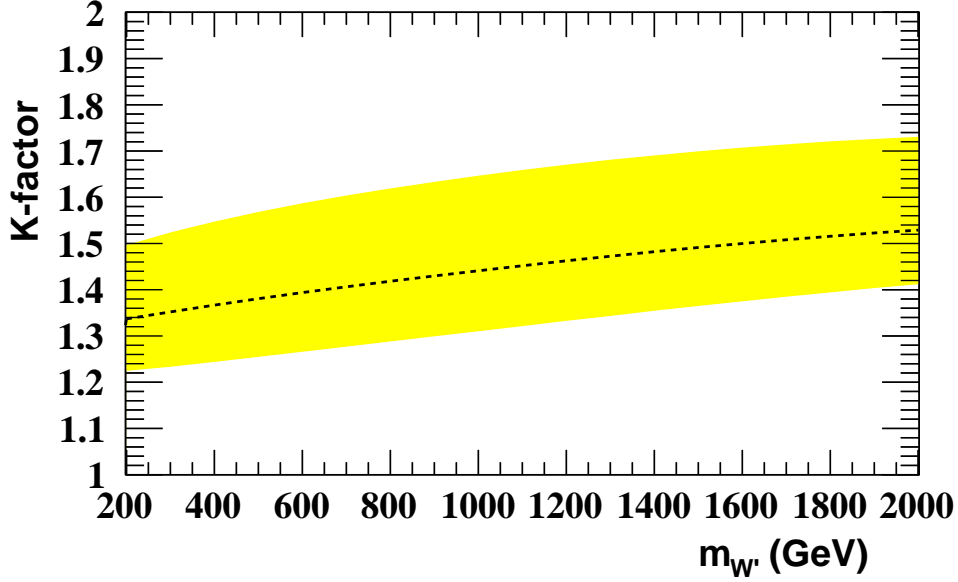


Figure 5: The K -factor for W' production as defined in eq. (3), with combined scale and PDF uncertainty.

figures 6 and 7 respectively, at both LO and NLO. We see in both cases that the total cross section is dominated by t quark production, due to the presence of valence rather than sea quarks in the initial state at LO. Furthermore, we note that the theoretical uncertainty is dominated by PDF uncertainties rather than scale variation, as the latter effect is similar for top and anti-top production, and cancels in the ratio.

The top quark fraction is higher for Z' rather than W' production, due to the dominance of up quarks over down quarks in the proton. Note that the fractions increase with the gauge boson mass, reflecting the fact that the partons are evaluated at higher x values on average as the gauge boson mass increases, which causes sea-quark dominated processes to fall off at the expense of those which are dominated by valence quarks. We may also note that the fraction changes slightly at NLO, and can either decrease or increase, depending on the gauge boson mass. This is due to two competing effects. Firstly, extra partonic subchannels open up at NLO which are insensitive to the exchange of a top and anti-top quark. This acts to decrease the fraction of top quark events. Secondly, the partons are evaluated at slightly higher x values at NLO compared to LO. This increases the dominance of valence quark-initiated processes, and acts to increase the proportion of top quark events. The size of the latter effect is somewhat uncertain due to the influence of high- x sea quark distributions. This can clearly be seen in both figures 6 and 7, where we show the top quark fraction for CTEQ as well as MSTW partons. The CTEQ results lead to higher top-quark fractions, with a decrease at NLO (apart from W' production at low gauge boson masses). In the MSTW results, there is an increase in the top-quark fraction at NLO, suggesting that valence quark distribution effects are more dominant.

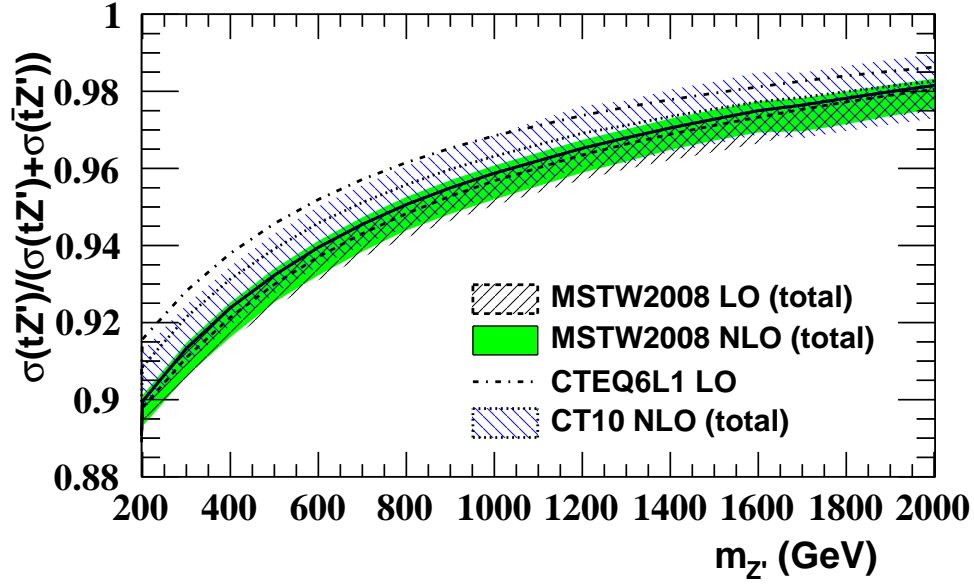


Figure 6: Fraction of Z' events containing a top (rather than anti-top) quark, together with combined scale and PDF uncertainties.

In this section, we have considered a subset of possible couplings in eq. (4), in particular considering only the $u - t$ and $d - t$ interactions for W' and Z' respectively. In the supplementary material, we present tables of results for other possible choices. Furthermore, we present results for the LHC at 8 TeV. Having discussed the total cross-section results in detail, we discuss NLO corrections to kinematic distributions of the top quark and gauge bosons in the following section.

4 Top and heavy gauge boson kinematics

In this section, we examine the impact of NLO QCD corrections on various kinematic distributions relating to the top quark and gauge boson. Throughout, we use the parameter choices described in the previous section, with MSTW LO and NLO partons [72] as appropriate.

In figure 8, we show the transverse-momentum and rapidity distributions for the top quark and gauge boson in tZ' production, for Z' masses of 200 GeV and 1000 GeV respectively. One sees that the top quark has a wide rapidity distribution peaking at zero, whereas the Z' boson is preferentially produced in either the forward or backward direction. This is due to the fact that we are here considering the case of production via coupling of the top to an up quark. The latter is a valence quark, and thus carries more momentum on average than the initial state gluon. This results in a boosted final state, where the Z' boson is preferentially emitted in the direction of the incoming up quark, from helicity considerations. The double peak structure will be absent for couplings between the top and second generation quarks, or for antitop production, as there is then no valence quark

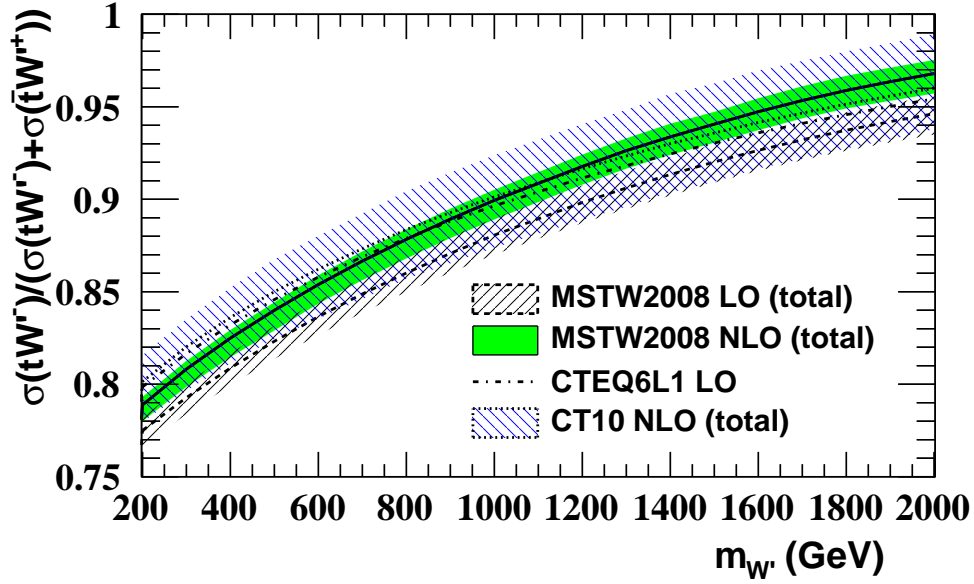


Figure 7: Fraction of W' events containing a top (rather than anti-top) quark, together with combined scale and PDF uncertainties.

in the initial state. Furthermore, the rapidity distributions become narrower as the gauge boson mass increases, reflecting the fact that production becomes more central for heavier final states. This is also reflected in the fact that the peaks of the transverse momentum distributions (for both the top quark and gauge boson) shift upwards as the gauge boson mass increases.

We show the ratio of the NLO and LO results for the above distributions for a 200 GeV gauge Z' boson in figure 9. One sees that for lower gauge boson masses, NLO corrections have little impact on the shape of the transverse momentum distributions of the top quark or Z' boson (although the tails of the NLO distributions are slightly softer, as expected). This can be understood by the fact that QCD radiation is dominated by emissions which are collinear to the incoming particles: the heavy final state limits the phase space for hard gluon emission, and contains a non-radiating colour-singlet particle and a heavy quark, such that there are no final state collinear singularities. This expectation is confirmed in figure 10, which shows the rapidity distribution of the additional parton emitted at NLO. The distribution is wide and flat, and thus characteristic of initial state radiation. This acts to make the rapidity distributions of the t and Z' more strongly peaked at central values (i.e. there is less energy available to the tZ' pair), and thus to proportionally reduce the double peak structure in the Z' -boson rapidity distribution. Ratio plots for a heavy gauge boson (1000 GeV) are also shown in figure 9. Here one sees that the transverse momentum of the top gets somewhat softer at NLO (more so than for lower gauge boson masses), and also its rapidity distribution is slightly less central. This can be understood by noting that the top quark is more energetic on average for heavier gauge boson masses, due to momentum conservation. It can therefore emit harder radiation, such that the jet and top quark are produced slightly off-centre.

This is borne out by the rapidity distribution of the extra parton in figure 10, which shows a shape difference with respect to the case of a 200 GeV boson.

Analogous results for tW' production are shown in figure 11, again for gauge boson masses of 200 GeV and 1000 GeV. Corresponding ratio plots are shown in figure 12. The results are broadly similar to the Z' results apart from one qualitative feature: the lack of a double peak in the W' -boson rapidity distribution. This is due to the fact that the initial state contains a down rather than an up quark, which carries proportionally less momentum, thus weakening the boost of the final state. A reasonable effect persists however, as can be seen by the fact that the W' rapidity distribution is noticeably wider than that of the top quark. Again, real emission corrections are dominated by initial state radiation, which is born out by the rapidity distribution of the extra parton in the lower panels of figure 10. There is again a difference in how rapidity distributions change at NLO in going from lower to higher gauge-boson masses, due to the fact that final-state radiation from the top is harder on average due to its recoiling against a highly massive boson.

In this and the previous section, we have examined the impact of NLO cross sections on total rates and distributions. A useful preliminary application of these results is to examine their impact on current searches for top-associated W' and Z' production. This is the subject of the following section.

5 Implications for tW' and tZ' searches

In this section we discuss the implications of our results for experimental searches. As a specific example, we consider the impact on results from a recent ATLAS search [74, 75] for tW' with $W' \rightarrow td$, in order to illustrate the impact of the results in this paper.

Experimental searches for tZ' or tW' production make use of LO Monte Carlo simulations, typically with events from the MADGRAPH [76] matrix element generator. We note that the latest release (2.6) of Herwig++ [77] also implements relevant models for tW' and tZ' . The cross-sections for the new-physics processes and kinematics of the top quark and associated heavy boson are generally derived from these LO codes. Correction of the cross section to the NLO values is straightforward using the results from Section 3 (see also the supplementary material for different coupling choices). Thus experimental upper limits on cross-sections correspond to stronger limits on the allowed couplings. Furthermore the reduced scale dependence at NLO means that a limit on the coupling that fully accounts for the uncertainty on the cross section would be substantially improved. The kinematics of the top and associated heavy boson can also be corrected to account for the differing distributions at NLO. We stress that, since at NLO the top and heavy boson are produced more centrally, the acceptance would be higher for events produced at NLO than LO. It is thus the case that using LO samples to derive acceptance and set upper limits on cross sections is a conservative approach.

The charge asymmetry in the production rate of the top quarks from heavy boson decays can also be exploited in a search. The SM $t\bar{t}$ +jet background is charge symmetric, so choosing to look at the anti-top+jet rather than top +jet mass spectrum can reduce the background by a factor of two while preserving the majority of signal. This is the case in the recent ATLAS search [75] where

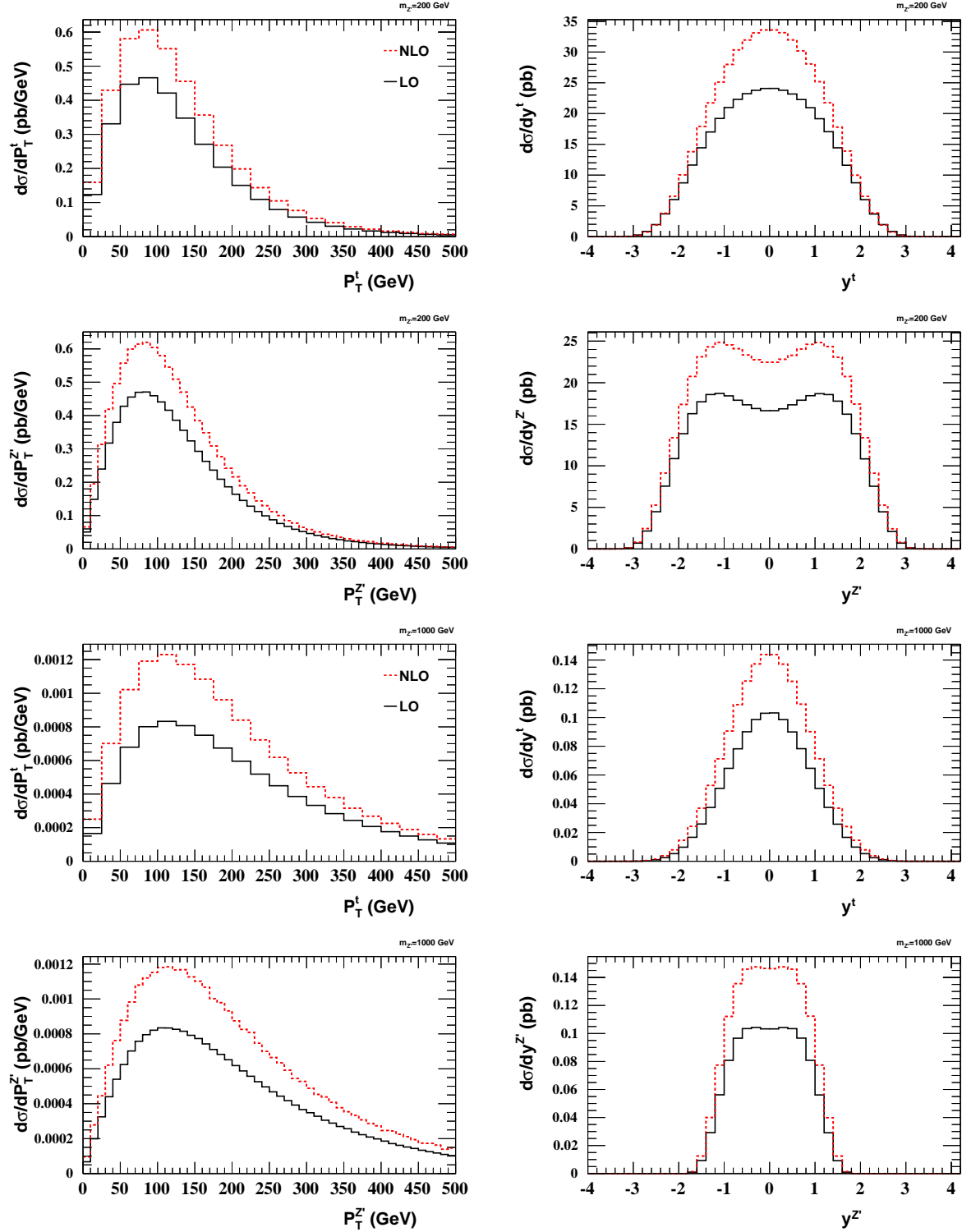


Figure 8: Transverse-momentum and rapidity distributions for the top quark and gauge boson in tZ' production for Z' masses of 200 GeV and 1000 GeV.

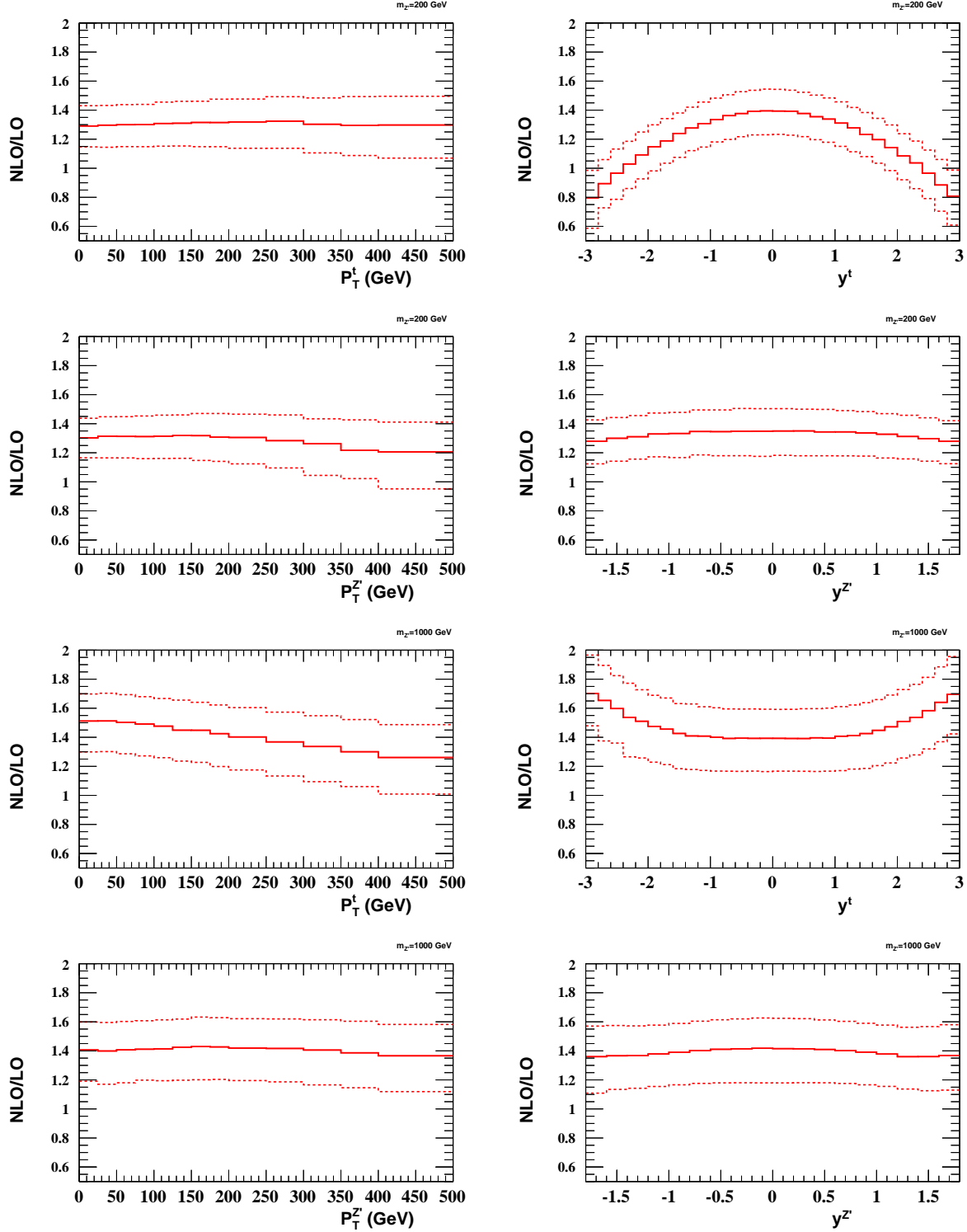


Figure 9: Ratio of the NLO and LO predictions for the transverse-momentum and rapidity distributions of the top quark and gauge boson in tZ' production with Z' masses of 200 GeV and 1000 GeV. The scale uncertainties are shown as dashed lines.

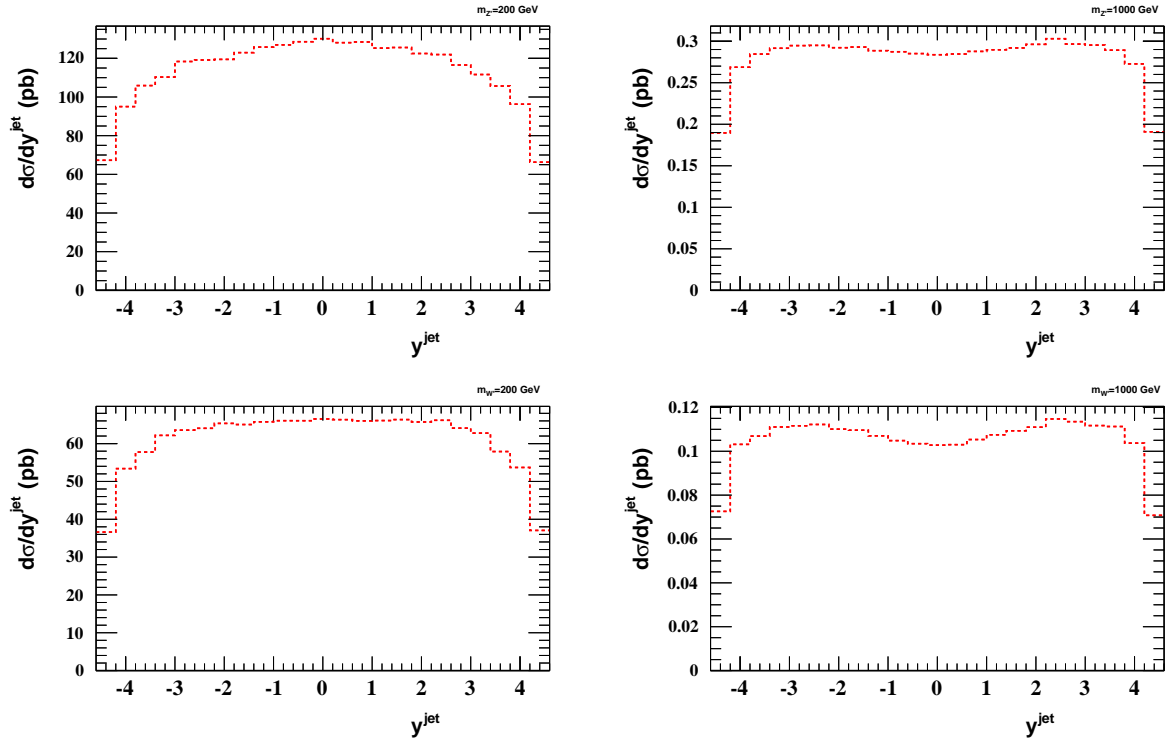


Figure 10: Rapidity distributions for the extra parton at NLO, for gauge boson masses of 200 GeV (left) and 1000 GeV (right), in Z' (upper) and W' (lower) production.

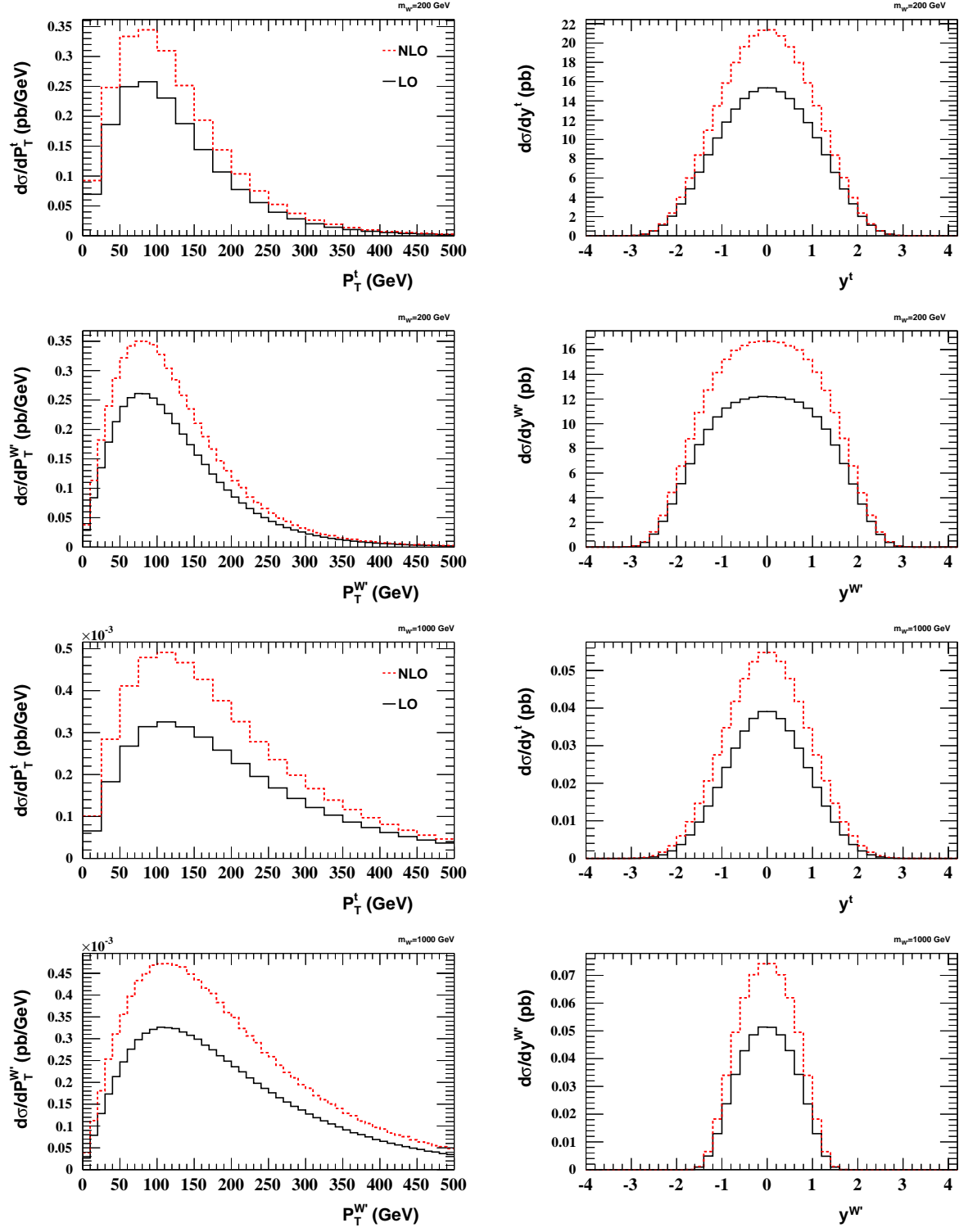


Figure 11: Transverse-momentum and rapidity distributions for the top quark and gauge boson in tW' production with W' masses 200 GeV and 1000 GeV.

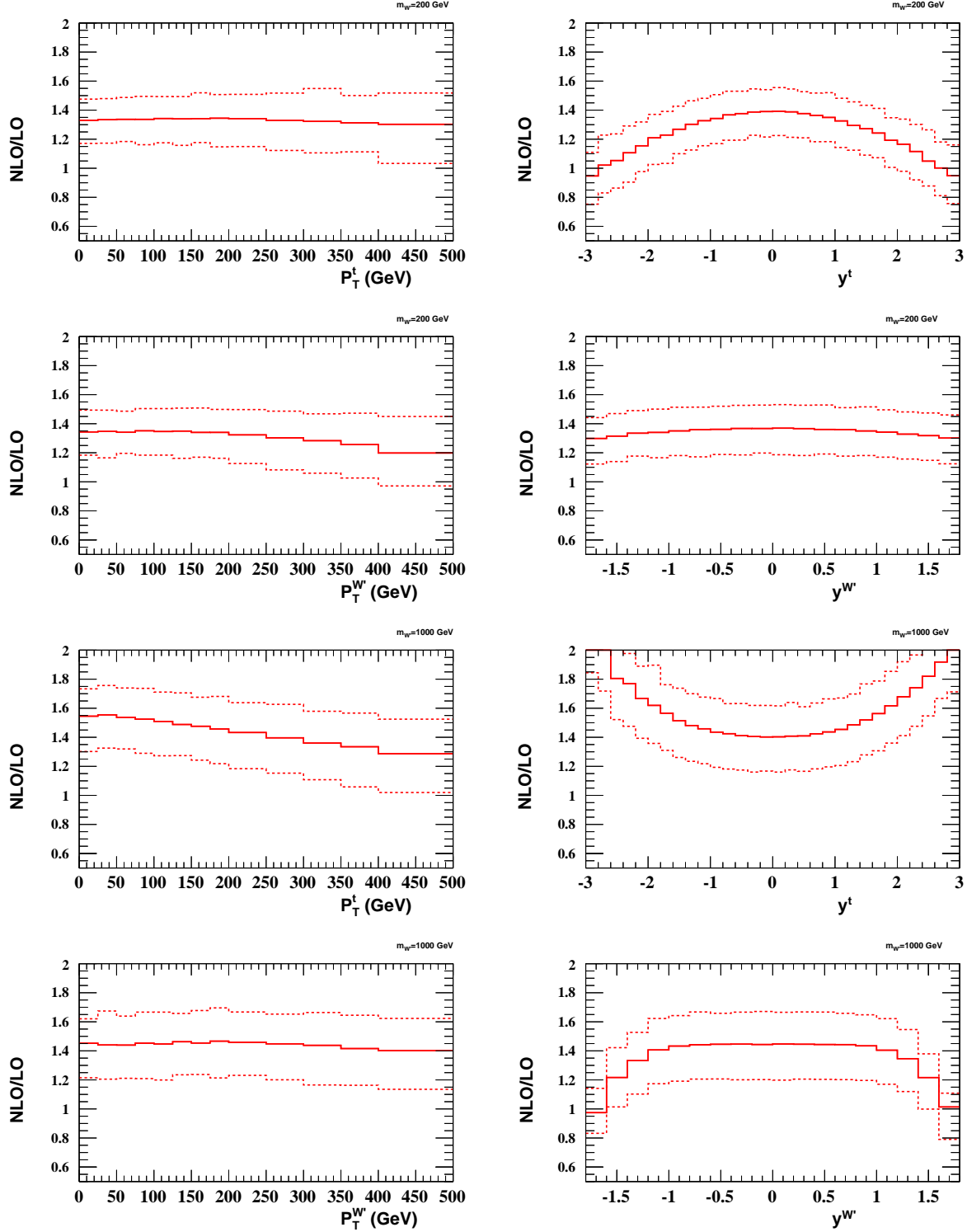


Figure 12: Ratio of NLO and LO predictions for the transverse-momentum and rapidity distributions for the top quark and gauge boson in tW' production for W' masses of 200 GeV and 1000 GeV. The scale uncertainties are shown as dashed lines.

windows in the top+jet mass vs anti-top+jet mass plane that give optimal sensitivity to signal are chosen. We showed in Section 3 that this asymmetry is quite stable in moving from LO to NLO and have provided the necessary information to account for this effect.

In order to demonstrate the impact of our NLO corrections, we first show in figure 13 a series of exclusion limits in the $(g_R, M_{W'})$ plane. The LO and NLO figures are obtained by taking the cross-section limit from the ATLAS search [74, 75], and using our LO and NLO calculations respectively, with scale choices and other parameters as defined in section 3. Also shown is the region favoured by the Tevatron forward-backward asymmetry measurements [8, 9], here taken from [75]. We see that NLO corrections significantly increase the constraints in parameter space, effectively cutting off most of the region that is still favoured by the Tevatron measurements. Whilst W' models do not have to explain the forward-backward asymmetry, this was a significant motivation for considering them in the first place. Thus, the fact that only a sliver of asymmetry-favoured space remains is an important result, justifying the calculation of NLO corrections.

A similar conclusion has been reached by the ATLAS collaboration itself, who have used the results of the present paper in their most up-to-date analysis [75]. Note that our NLO exclusion limits differ slightly from theirs, due to the fact that it has been calculated independently, using estimates of the cross-section limits presented in [74, 75]. Also, we have here used a default common factorisation and renormalisation scale of $(m_t + m_X)/2$, as opposed to the fixed scale of 200 GeV used by ATLAS for their LO limit [74]. We do not see a motivation for the latter scale for high gauge boson masses. Nevertheless, the results are broadly similar to those of [75].

The CMS collaboration have also presented bounds on W' production [52]. However, unlike the ATLAS analysis, this bound is on the combination of the resonant $W't$ process, and the t -channel exchange process. One could take this to be a conservative estimate on the resonant process, but this would give a much weaker bound on the $W't$ cross-section than would be obtained in practice. For this reason, we do not show the CMS result in figure 13, so as not to introduce an unfair comparison. Another reason for not including this is a recent study [78] showing that interference with SM $t\bar{t}$ + jet production is important for the CMS search, and significantly weakens the limit. The effect of such interference is negligible for searches that focus on the resonant $W't$ process.

Note that our analysis in this section is only an approximate estimate of the exclusion limits implied by our NLO calculation. Firstly, and as stated above, we have not taken into account explicitly that the theoretical uncertainty of the NLO cross-section (due predominantly to scale variation) is significantly reduced relative to LO. Secondly, we have not accounted for the change in kinematic distributions, which would affect the acceptance. There is also an important interplay between these direct searches and additional constraints such as those discussed in the introduction. A more realistic analysis can be found in the ATLAS paper [75], but we think it still worth presenting an independent exclusion plot here. Firstly, it is interesting to note that a rough estimate gives results which are reasonably similar to the ATLAS analysis. Secondly, we use a more physically motivated scale choice, which can be much different to the fixed LO scale of 200 GeV used by [29] and the ATLAS analysis, at high gauge boson masses. It is reassuring to see that this does not lead to a large deviation from their results.

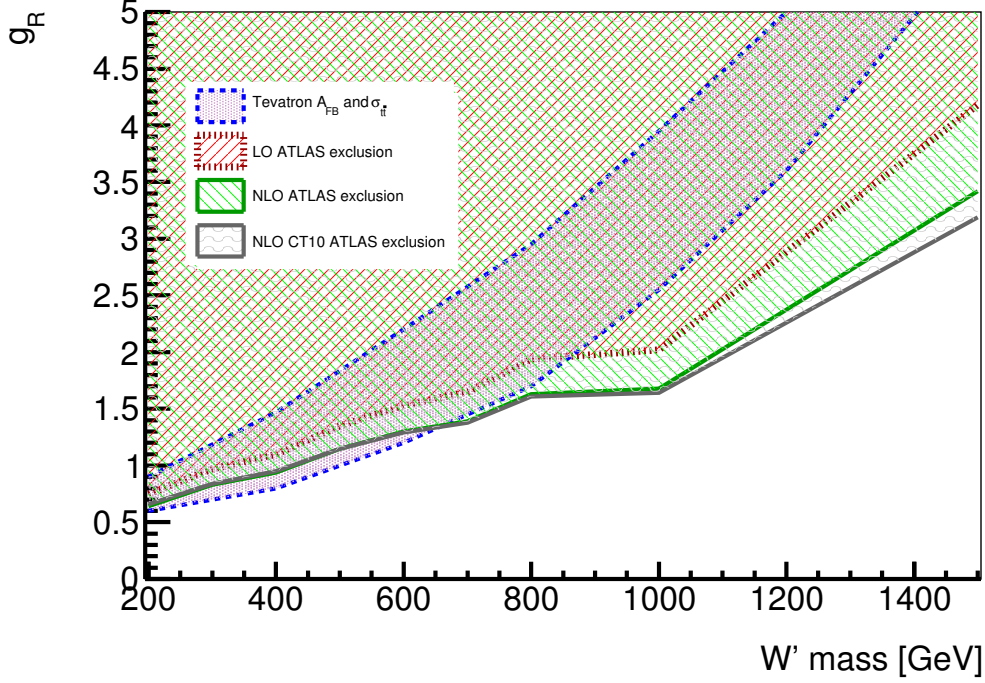


Figure 13: Example of the strengthening of constraints on the coupling g_R when taking the NLO corrections to tW' production into account. The LO exclusion curve is made using the calculations with the MSTW2008 LO PDF set. The NLO curves are made using the calculations with the MSTW2008 LO and CT10 PDF sets.

In this section, we have illustrated the impact of our NLO results in the well-studied case (both theoretically and experimentally) in which the top couples to the first generation quarks only. It is worth stressing that our NLO calculation would also be useful in scenarios with alternative coupling choices, where their impact may be larger.

6 Conclusion

In this paper, we have calculated NLO QCD corrections to the associated production of W' and Z' boson production with a top quark. This production mode is being actively searched for by both the ATLAS and CMS collaborations, and higher-order corrections are important in order to set tight bounds on couplings and gauge boson masses, due to both the size of NLO effects, and the requisite reduction in theoretical uncertainty. As we have seen, for models in which the top quark couples to first generation quarks, the uncertainty is dominated by scale variation, whereas the PDF uncertainty is small, due to the fact that high- x valence quark distributions are well-constrained in global fits. One thus achieves a significant decrease in theoretical uncertainty in going to NLO, as can be seen directly in the total cross-section plots of figures 2 and 3.

Although we have focussed on the particular Lagrangian of eq. (4), our analysis is more general in

that one can straightforwardly combine the results collected in the main body of this paper and the supplementary material in order to generate total cross sections for models which have non-trivial mixing between quark generations or a mixture of left- and right-handed couplings. Thus, our results can be directly and generally applied in current experimental analyses, which may differ somewhat in the particular models which are being considered. Our aim has been to provide as complete a set of numbers as possible for use in experimental searches, including cross sections at a centre-of-mass energy of 8 TeV, which can be found in the supplementary material. Results for alternative parameter choices, if desired, may be requested by contacting the authors.

As well as total cross-sections, we also considered transverse momentum and rapidity distributions of the top quark and gauge bosons. We find that NLO corrections lead, predictably, to a softening of transverse momentum distributions, which effect increases with the gauge boson mass. Rapidity distributions are more affected even at low gauge boson masses, due to the fact that real emission corrections are dominated by initial state radiation. The top quark becomes more (less) central at low (high) gauge boson masses.

In section 5, we briefly examined the implications of our results for current searches, and estimated how coupling and mass limits would change in the recently presented ATLAS analysis of [75]. We find that coupling bounds are strengthened by around 20%, and that the region favoured by the Tevatron forward-backward asymmetry is all but excluded. The latter is a significant result, given that this asymmetry is a major motivation for considering W' and Z' models in the first place. Our analysis is an approximate estimate, and could be enhanced by taking into account the fact that the theoretical uncertainty diminishes when NLO corrections are implemented, and that kinematic distributions change (affecting the acceptance of signal events).

To summarise, we have provided NLO QCD corrections for use in experimental searches for Z' and W' bosons in association with a top quark. The hunt for such particles is ongoing.

Acknowledgements

This work was supported in part by grant DE-FG02-92ER40704 from the U.S. Dept. of Energy. We thank Daniel Whiteson for discussions and comments on the manuscript and Steven Worm for discussions regarding the CMS limits. JA thanks Moira I. Gresham, Ian-Woo Kim and Kathryn M. Zurek for useful discussions about the tW' and tZ' models. JF is supported by the UK Science and Technology Facilities Council (STFC). CDW thanks Stefano Frixione for useful conversations, and also David Miller for discussions. He is supported by the STFC Postdoctoral Fellowship ‘‘Collider Physics at the LHC’’.

A Supplementary material

In this supplementary material, we collect various additional results from our NLO W' and Z' calculation, which are of further use for current (and future) experimental analyses. As in the main paper, we adopt the Lagrangians

$$\begin{aligned}\mathcal{L}_{W'} &= \frac{P_{tD}}{\sqrt{2}} \bar{D} \gamma^\mu g_R P_R t W' + \text{h.c.}; \\ \mathcal{L}_{Z'} &= \frac{Q_{tU}}{\sqrt{2}} \bar{U} \gamma^\mu g_R P_R t Z' + \text{h.c.},\end{aligned}\tag{4}$$

where P_{tD} and Q_{tU} are suitable mixing matrices. The main paper focuses on the cases $P_{td} = Q_{tU} = 1$ (all other $P_{ij} = Q_{ij} = 0$). Here we consider other possible coupling choices, and also how to combine these in order to obtain total NLO cross-sections in general models. For completeness, we also give results for t and \bar{t} production separately, beginning in the following section.

A.1 Cross-section results at 7 TeV separated by top charge

This section contains the total cross sections for t and \bar{t} production separately. These are for cases where the Z' (W') couples to tu (td). For couplings to second and third generation quarks, no charge asymmetry is expected due to the equality $q(x) = \bar{q}(x)$ for sea quark distributions⁵).

Tables 5 and 6 give the cross sections at LO for tZ' production where the t is specifically a top quark and anti-top quark respectively. The NLO cross sections for the same process are given in Tables 7 and 8. The equivalent cross sections for tW' production are given in Tables 9-12.

A.2 Cross-section results for other partonic couplings

In the main paper, we have explicitly analysed the Lagrangian of eq (4), with the only non-zero couplings being those between the third and first quark generations ($P_{td} = Q_{tu} = 1$). In this appendix, we collect total cross-sections for alternative coupling choices, before discussing how these results can be combined in the general case.

In tables 13-16 we present total LO and NLO cross-sections for tW' production for the choices $P_{ts} = 1$ and, separately, $P_{tb} = 1$ (all other P_{tD} zero in each case). Similarly, the total cross-section for tZ' production at LO and NLO is shown in tables 17 and 18 for $Q_{tc} = 1$ (all other Q_{tU} zero). Some comments are in order regarding a couple of features noticeable in the results. Firstly, the K -factor for both W' and Z' production decreases with increasing gauge boson mass for the MSTW parton choice. This is a reflection of the fact that the initial state involves only gluons and sea quark (or heavy flavour) distributions. As the final state gets heavier, these distributions are probed at higher x values, where they fall off rapidly. This effect is most pronounced for Z' production with a tc coupling, where the K factor becomes less than one at the highest gauge boson masses. Secondly, the K factor results show much more variation when CTEQ6L1 and CT10 partons are used, including wider disagreements with the MSTW results. We put this down to the fact that CTEQ substantially revised their treatment of heavy flavour effects from CTEQ6.5 onwards [81]. One

⁵Modern PDF analyses typically allow $s(x) \neq \bar{s}(x)$ [72, 79, 80]. However, this would result in a negligible charge asymmetry.

| $M(Z') \text{ (GeV)}$ | $\sigma_{\text{born}}^{\text{CTEQ6L1}}(\bar{t}Z') \text{ (pb)}$ | $\sigma_{\text{born}}^{\text{MSTW 2008 LO}}(\bar{t}Z') \text{ (pb)}$ |
|-----------------------|---|--|
| 200 | 6.51 +1.42 -1.08 | 8.04 +1.85 -1.40 |
| 300 | 1.89 +0.44 -0.33 | 2.41 +0.59 -0.44 |
| 400 | 0.66 +0.16 -0.12 | 0.87 +0.23 -0.17 |
| 500 | 0.262 +0.066 -0.049 | 0.353 +0.096 -0.070 |
| 600 | 0.113 +0.029 -0.022 | 0.156 +0.044 -0.032 |
| 700 | 0.052 +0.014 -0.010 | 0.073 +0.021 -0.015 |
| 800 | 0.0251 +0.0069 -0.0050 | 0.0363 +0.0109 -0.0077 |
| 900 | 0.0126 +0.0035 -0.0026 | 0.0187 +0.0057 -0.0041 |
| 1000 | 0.0066 +0.0019 -0.0014 | 0.0099 +0.0031 -0.0022 |
| 1100 | 0.0035 +0.0010 -0.0007 | 0.0054 +0.0017 -0.0012 |
| 1200 | 0.00193 +0.00056 -0.00040 | 0.00299 +0.00099 -0.00069 |
| 1300 | 0.00107 +0.00032 -0.00023 | 0.00169 +0.00057 -0.00040 |
| 1400 | 0.00061 +0.00018 -0.00013 | 0.00097 +0.00034 -0.00023 |
| 1500 | 0.00035 +0.00011 -0.00008 | 0.00056 +0.00020 -0.00014 |
| 1600 | 0.00020 +0.00006 -0.00004 | 0.00033 +0.00012 -0.00008 |
| 1700 | 0.000117 +0.000037 -0.000026 | 0.000195 +0.000071 -0.000048 |
| 1800 | 0.000069 +0.000022 -0.000015 | 0.000116 +0.000043 -0.000029 |
| 1900 | 0.000041 +0.000013 -0.000009 | 0.000069 +0.000026 -0.000018 |
| 2000 | 0.000024 +0.000008 -0.000006 | 0.000041 +0.000016 -0.000011 |

Table 5: Leading order cross sections for $pp \rightarrow \bar{t}Z'$ at the 7 TeV LHC.

| $M(Z') \text{ (GeV)}$ | $\sigma_{\text{born}}^{\text{CTEQ6L1}}(tZ') \text{ (pb)}$ | $\sigma_{\text{born}}^{\text{MSTW 2008 LO}}(tZ') \text{ (pb)}$ |
|-----------------------|---|--|
| 200 | 71.3 +14.9 -11.4 | 71.2 +15.5 -11.8 |
| 300 | 24.74 +5.49 -4.17 | 24.85 +5.78 -4.34 |
| 400 | 10.14 +2.36 -1.77 | 10.27 +2.51 -1.87 |
| 500 | 4.62 +1.12 -0.83 | 4.73 +1.21 -0.89 |
| 600 | 2.27 +0.57 -0.42 | 2.35 +0.62 -0.45 |
| 700 | 1.181 +0.302 -0.223 | 1.232 +0.336 -0.245 |
| 800 | 0.641 +0.168 -0.123 | 0.676 +0.190 -0.137 |
| 900 | 0.360 +0.096 -0.070 | 0.383 +0.111 -0.080 |
| 1000 | 0.208 +0.057 -0.041 | 0.224 +0.066 -0.047 |
| 1100 | 0.123 +0.034 -0.025 | 0.133 +0.040 -0.029 |
| 1200 | 0.0739 +0.0208 -0.0151 | 0.0809 +0.0251 -0.0177 |
| 1300 | 0.0451 +0.0129 -0.0093 | 0.0499 +0.0158 -0.0111 |
| 1400 | 0.0279 +0.0081 -0.0058 | 0.0311 +0.0101 -0.0070 |
| 1500 | 0.0175 +0.0051 -0.0037 | 0.0196 +0.0065 -0.0045 |
| 1600 | 0.0110 +0.0033 -0.0024 | 0.0125 +0.0042 -0.0029 |
| 1700 | 0.0070 +0.0021 -0.0015 | 0.0080 +0.0027 -0.0019 |
| 1800 | 0.00448 +0.00137 -0.00097 | 0.00515 +0.00179 -0.00123 |
| 1900 | 0.00288 +0.00089 -0.00063 | 0.00333 +0.00118 -0.00081 |
| 2000 | 0.00186 +0.00058 -0.00041 | 0.00216 +0.00078 -0.00053 |

Table 6: Leading order cross sections for $pp \rightarrow tZ'$ at the 7 TeV LHC.

| $M(Z') \text{ (GeV)}$ | $\sigma_{\text{nlo}}^{\text{CT10}}(\bar{t}Z') \text{ (pb)}$ | | | $\sigma_{\text{nlo}}^{\text{MSTW 2008 NLO}}(\bar{t}Z') \text{ (pb)}$ | | |
|-----------------------|---|------------------------|------------------------|--|------------------------|------------------------|
| 200 | 9.17 | +0.60 -0.66 | +0.80 -0.89 | 10.31 | +0.70 -0.77 | +0.35 -0.32 |
| 300 | 2.74 | +0.18 -0.21 | +0.29 -0.31 | 3.09 | +0.21 -0.24 | +0.13 -0.12 |
| 400 | 0.99 | +0.07 -0.08 | +0.13 -0.13 | 1.12 | +0.08 -0.09 | +0.06 -0.05 |
| 500 | 0.402 | +0.028 -0.033 | +0.061 -0.057 | 0.457 | +0.033 -0.039 | +0.027 -0.025 |
| 600 | 0.178 | +0.013 -0.015 | +0.032 -0.028 | 0.203 | +0.016 -0.018 | +0.014 -0.013 |
| 700 | 0.085 | +0.007 -0.008 | +0.018 -0.015 | 0.096 | +0.008 -0.009 | +0.008 -0.007 |
| 800 | 0.0422 | +0.0034 -0.0040 | +0.0100 -0.0082 | 0.0479 | +0.0040 -0.0046 | +0.0042 -0.0039 |
| 900 | 0.0219 | +0.0018 -0.0021 | +0.0059 -0.0046 | 0.0248 | +0.0022 -0.0025 | +0.0024 -0.0023 |
| 1000 | 0.0118 | +0.0010 -0.0012 | +0.0036 -0.0027 | 0.0132 | +0.0012 -0.0014 | +0.0014 -0.0013 |
| 1100 | 0.0065 | +0.0006 -0.0007 | +0.0022 -0.0016 | 0.0073 | +0.0007 -0.0008 | +0.0009 -0.0008 |
| 1200 | 0.0037 | +0.0004 -0.0004 | +0.0014 -0.0010 | 0.0041 | +0.0004 -0.0005 | +0.0005 -0.0005 |
| 1300 | 0.00210 | +0.00021 -0.00023 | +0.00091 -0.00061 | 0.00231 | +0.00024 -0.00027 | +0.00033 -0.00031 |
| 1400 | 0.00123 | +0.00013 -0.00014 | +0.00059 -0.00039 | 0.00134 | +0.00014 -0.00016 | +0.00021 -0.00019 |
| 1500 | 0.00073 | +0.00008 -0.00009 | +0.00039 -0.00024 | 0.00078 | +0.00009 -0.00010 | +0.00013 -0.00012 |
| 1600 | 0.00043 | +0.00005 -0.00005 | +0.00026 -0.00016 | 0.00046 | +0.00005 -0.00006 | +0.00008 -0.00008 |
| 1700 | 0.000262 | +0.000030 -0.000033 | +0.000174 -0.000101 | 0.000272 | +0.000033 -0.000035 | +0.000052 -0.000049 |
| 1800 | 0.000159 | +0.000019 -0.000021 | +0.000118 -0.000065 | 0.000162 | +0.000020 -0.000021 | +0.000033 -0.000031 |
| 1900 | 0.000097 | +0.000012 -0.000013 | +0.000080 -0.000042 | 0.000097 | +0.000013 -0.000013 | +0.000021 -0.000020 |
| 2000 | 0.000060 | +0.000008 -0.000008 | +0.000055 -0.000028 | 0.000058 | +0.000008 -0.000008 | +0.000014 -0.000012 |

Table 7: Next-to-leading order cross sections for $pp \rightarrow \bar{t}Z'$ at the 7 TeV LHC.

| $M(Z') \text{ (GeV)}$ | $\sigma_{\text{nlo}}^{\text{CT10}}(tZ') \text{ (pb)}$ | | | $\sigma_{\text{nlo}}^{\text{MSTW 2008 NLO}}(tZ') \text{ (pb)}$ | | |
|-----------------------|---|----------------------|----------------------|--|----------------------|----------------------|
| 200 | 92.0 | +6.1 -6.5 | +2.4 -2.6 | 93.1 | +6.4 -6.7 | +1.1 -0.7 |
| 300 | 32.55 | +2.13 -2.38 | +0.99 -1.01 | 32.97 | +2.23 -2.47 | +0.37 -0.26 |
| 400 | 13.60 | +0.90 -1.04 | +0.51 -0.49 | 13.78 | +0.94 -1.07 | +0.17 -0.13 |
| 500 | 6.33 | +0.43 -0.50 | +0.29 -0.27 | 6.40 | +0.45 -0.52 | +0.09 -0.07 |
| 600 | 3.17 | +0.22 -0.26 | +0.18 -0.16 | 3.21 | +0.23 -0.27 | +0.06 -0.05 |
| 700 | 1.682 | +0.122 -0.145 | +0.111 -0.100 | 1.698 | +0.127 -0.149 | +0.034 -0.029 |
| 800 | 0.932 | +0.070 -0.083 | +0.072 -0.064 | 0.938 | +0.073 -0.085 | +0.022 -0.019 |
| 900 | 0.534 | +0.042 -0.049 | +0.048 -0.042 | 0.536 | +0.043 -0.050 | +0.015 -0.013 |
| 1000 | 0.315 | +0.026 -0.030 | +0.032 -0.028 | 0.315 | +0.026 -0.031 | +0.010 -0.009 |
| 1100 | 0.190 | +0.016 -0.019 | +0.022 -0.019 | 0.189 | +0.016 -0.019 | +0.007 -0.006 |
| 1200 | 0.117 | +0.010 -0.012 | +0.016 -0.013 | 0.115 | +0.010 -0.012 | +0.005 -0.004 |
| 1300 | 0.0730 | +0.0067 -0.0076 | +0.0112 -0.0087 | 0.0716 | +0.0067 -0.0076 | +0.0032 -0.0029 |
| 1400 | 0.0462 | +0.0044 -0.0050 | +0.0080 -0.0060 | 0.0450 | +0.0044 -0.0049 | +0.0022 -0.0020 |
| 1500 | 0.0296 | +0.0029 -0.0033 | +0.0058 -0.0042 | 0.0285 | +0.0029 -0.0032 | +0.0015 -0.0014 |
| 1600 | 0.0191 | +0.0019 -0.0022 | +0.0042 -0.0030 | 0.0182 | +0.0019 -0.0021 | +0.0011 -0.0010 |
| 1700 | 0.0124 | +0.0013 -0.0015 | +0.0031 -0.0021 | 0.0117 | +0.0013 -0.0014 | +0.0007 -0.0007 |
| 1800 | 0.0081 | +0.0009 -0.00010 | +0.0023 -0.0015 | 0.0076 | +0.0009 -0.0009 | +0.0005 -0.0005 |
| 1900 | 0.00536 | +0.00061 -0.00066 | +0.00167 -0.00105 | 0.00494 | +0.00057 -0.00062 | +0.00036 -0.00034 |
| 2000 | 0.00354 | +0.00042 -0.00045 | +0.00123 -0.00075 | 0.00322 | +0.00039 -0.00041 | +0.00025 -0.00024 |

Table 8: Next-to-leading order cross sections for $pp \rightarrow tZ'$ at the 7 TeV LHC.

| $M(W'^+) \text{ (GeV)}$ | $\sigma_{\text{born}}^{\text{CTEQ6L1}}(\bar{t}W'^+) \text{ (pb)}$ | $\sigma_{\text{born}}^{\text{MSTW 2008 LO}}(\bar{t}W'^+) \text{ (pb)}$ |
|-------------------------|---|--|
| 200 | 8.40 +1.88 -1.42 | 9.58 +2.27 -1.70 |
| 300 | 2.49 +0.59 -0.44 | 2.88 +0.73 -0.54 |
| 400 | 0.88 +0.22 -0.16 | 1.03 +0.28 -0.20 |
| 500 | 0.350 +0.091 -0.067 | 0.414 +0.116 -0.084 |
| 600 | 0.151 +0.040 -0.030 | 0.180 +0.053 -0.038 |
| 700 | 0.0692 +0.019 -0.014 | 0.083 +0.025 -0.018 |
| 800 | 0.0333 +0.0094 -0.0068 | 0.0403 +0.0126 -0.0089 |
| 900 | 0.0166 +0.0048 -0.0034 | 0.0202 +0.0065 -0.0045 |
| 1000 | 0.0085 +0.0025 -0.0018 | 0.0104 +0.0034 -0.0024 |
| 1100 | 0.0045 +0.0013 -0.0010 | 0.0055 +0.0019 -0.0013 |
| 1200 | 0.00240 +0.00072 -0.00052 | 0.00295 +0.00102 -0.00070 |
| 1300 | 0.00131 +0.00040 -0.00028 | 0.00161 +0.00057 -0.00039 |
| 1400 | 0.00072 +0.00022 -0.00016 | 0.00089 +0.00032 -0.00022 |
| 1500 | 0.00040 +0.00013 -0.00009 | 0.00050 +0.00018 -0.00012 |
| 1600 | 0.00023 +0.00007 -0.00005 | 0.00028 +0.00010 -0.00007 |
| 1700 | 0.000127 +0.000041 -0.000029 | 0.000159 +0.000060 -0.000040 |
| 1800 | 0.000072 +0.000023 -0.000016 | 0.000091 +0.000035 -0.000023 |
| 1900 | 0.000041 +0.000014 -0.000009 | 0.000052 +0.000020 -0.000014 |
| 2000 | 0.000023 +0.000008 -0.000005 | 0.000030 +0.000012 -0.000008 |

Table 9: Leading order cross sections for $pp \rightarrow \bar{t}W'^+$ at the 7 TeV LHC.

| $M(W'^-) \text{ (GeV)}$ | $\sigma_{\text{born}}^{\text{CTEQ6L1}}(tW'^-) \text{ (pb)}$ | $\sigma_{\text{born}}^{\text{MSTW 2008 LO}}(tW'^-) \text{ (pb)}$ |
|-------------------------|---|--|
| 200 | 33.4 +7.3 -5.5 | 33.1 +7.6 -5.7 |
| 300 | 11.11 +2.56 -1.93 | 11.04 +2.68 -2.00 |
| 400 | 4.381 +1.06 -0.79 | 4.38 +1.12 -0.82 |
| 500 | 1.93 +0.48 -0.36 | 1.94 +0.52 -0.38 |
| 600 | 0.916 +0.236 -0.174 | 0.928 +0.256 -0.186 |
| 700 | 0.461 +0.122 -0.089 | 0.470 +0.134 -0.097 |
| 800 | 0.243 +0.066 -0.048 | 0.249 +0.073 -0.052 |
| 900 | 0.133 +0.037 -0.027 | 0.137 +0.041 -0.029 |
| 1000 | 0.0743 +0.0209 -0.0151 | 0.0774 +0.0239 -0.0169 |
| 1100 | 0.0427 +0.0122 -0.0088 | 0.0447 +0.0141 -0.0099 |
| 1200 | 0.0250 +0.0072 -0.0052 | 0.0263 +0.0085 -0.0059 |
| 1300 | 0.0148 +0.0044 -0.0031 | 0.0157 +0.0052 -0.0036 |
| 1400 | 0.0089 +0.0027 -0.0019 | 0.0095 +0.0032 -0.0022 |
| 1500 | 0.00543 +0.00164 -0.00117 | 0.00580 +0.00199 -0.00137 |
| 1600 | 0.00333 +0.00102 -0.00072 | 0.00357 +0.00125 -0.00086 |
| 1700 | 0.00206 +0.00064 -0.00045 | 0.00221 +0.00079 -0.00054 |
| 1800 | 0.00128 +0.00040 -0.00028 | 0.00138 +0.00050 -0.00034 |
| 1900 | 0.00080 +0.00025 -0.00018 | 0.00086 +0.00032 -0.00022 |
| 2000 | 0.00050 +0.00016 -0.00011 | 0.00054 +0.00020 -0.00014 |

Table 10: Leading order cross sections for $pp \rightarrow tW'^-$ at the 7 TeV LHC.

| $M(W'^+) \text{ (GeV)}$ | $\sigma_{\text{nlo}}^{\text{CT10}}(\bar{t}W'^+) \text{ (pb)}$ | | | $\sigma_{\text{nlo}}^{\text{MSTW 2008 NLO}}(\bar{t}W'^+) \text{ (pb)}$ | | |
|-------------------------|---|------------------------|------------------------|--|------------------------|------------------------|
| 200 | 11.0 | +0.7 -0.8 | +1.0 -1.3 | 12.0 | +0.8 -0.9 | +0.4 -0.4 |
| 300 | 3.30 | +0.22 -0.26 | +0.37 -0.44 | 3.59 | +0.25 -0.29 | +0.15 -0.15 |
| 400 | 1.19 | +0.08 -0.10 | +0.16 -0.18 | 1.29 | +0.09 -0.11 | +0.06 -0.06 |
| 500 | 0.483 | +0.035 -0.041 | +0.076 -0.084 | 0.516 | +0.039 -0.046 | +0.029 -0.029 |
| 600 | 0.213 | +0.016 -0.019 | +0.039 -0.041 | 0.224 | +0.018 -0.021 | +0.014 -0.015 |
| 700 | 0.100 | +0.008 -0.009 | +0.021 -0.022 | 0.103 | +0.009 -0.010 | +0.008 -0.008 |
| 800 | 0.049 | +0.004 -0.005 | +0.012 -0.012 | 0.050 | +0.004 -0.005 | +0.004 -0.004 |
| 900 | 0.0249 | +0.0022 -0.0025 | +0.0072 -0.0066 | 0.0247 | +0.0023 -0.0026 | +0.0023 -0.0023 |
| 1000 | 0.0131 | +0.0012 -0.0014 | +0.0044 -0.0038 | 0.0126 | +0.0012 -0.0014 | +0.0013 -0.0013 |
| 1100 | 0.0070 | +0.0007 -0.0008 | +0.0027 -0.0022 | 0.0066 | +0.0007 -0.0008 | +0.0008 -0.0008 |
| 1200 | 0.0039 | +0.0004 -0.0004 | +0.0017 -0.0013 | 0.0035 | +0.0004 -0.0004 | +0.0005 -0.0005 |
| 1300 | 0.00215 | +0.00023 -0.00025 | +0.00108 -0.00081 | 0.00187 | +0.00021 -0.00023 | +0.00027 -0.00027 |
| 1400 | 0.00121 | +0.00013 -0.00015 | +0.00069 -0.00050 | 0.00101 | +0.00012 -0.00013 | +0.00017 -0.00016 |
| 1500 | 0.00069 | +0.00008 -0.00009 | +0.00045 -0.00031 | 0.00055 | +0.00007 -0.00007 | +0.00010 -0.00010 |
| 1600 | 0.00040 | +0.00005 -0.00005 | +0.00029 -0.00019 | 0.00030 | +0.00004 -0.00004 | +0.00006 -0.00006 |
| 1700 | 0.000230 | +0.000029 -0.000031 | +0.000194 -0.000120 | 0.000165 | +0.000022 -0.000023 | +0.000039 -0.000037 |
| 1800 | 0.000134 | +0.000017 -0.000018 | +0.000128 -0.000075 | 0.000091 | +0.000013 -0.000013 | +0.000024 -0.000023 |
| 1900 | 0.000078 | +0.000011 -0.000011 | +0.000085 -0.000047 | 0.000050 | +0.000007 -0.000007 | +0.000015 -0.000014 |
| 2000 | 0.000046 | +0.000006 -0.000007 | +0.000057 -0.000030 | 0.000027 | +0.000004 -0.000004 | +0.000009 -0.000009 |

Table 11: Next-to-leading order cross sections for $pp \rightarrow \bar{t}W'^+$ at the 7 TeV LHC.

| $M(W'^-) \text{ (GeV)}$ | $\sigma_{\text{nlo}}^{\text{CT10}}(tW'^-) \text{ (pb)}$ | | | $\sigma_{\text{nlo}}^{\text{MSTW 2008 NLO}}(tW'^-) \text{ (pb)}$ | | |
|-------------------------|---|----------------------|----------------------|--|----------------------|----------------------|
| 200 | 44.6 | +3.0 -3.2 | +2.1 -2.0 | 45.0 | +3.1 -3.4 | +0.6 -0.6 |
| 300 | 15.16 | +1.00 -1.14 | +0.81 -0.77 | 15.22 | +1.05 -1.18 | +0.23 -0.23 |
| 400 | 6.12 | +0.41 -0.48 | +0.38 -0.35 | 6.10 | +0.43 -0.49 | +0.10 -0.11 |
| 500 | 2.76 | +0.19 -0.23 | +0.20 -0.18 | 2.73 | +0.20 -0.23 | +0.05 -0.06 |
| 600 | 1.341 | +0.097 -0.115 | +0.113 -0.099 | 1.320 | +0.099 -0.116 | +0.030 -0.031 |
| 700 | 0.692 | +0.052 -0.061 | +0.067 -0.058 | 0.676 | +0.053 -0.062 | +0.018 -0.018 |
| 800 | 0.374 | +0.029 -0.034 | +0.041 -0.035 | 0.361 | +0.029 -0.034 | +0.011 -0.011 |
| 900 | 0.209 | +0.017 -0.020 | +0.026 -0.022 | 0.200 | +0.017 -0.020 | +0.007 -0.007 |
| 1000 | 0.120 | +0.010 -0.012 | +0.017 -0.014 | 0.114 | +0.010 -0.012 | +0.005 -0.005 |
| 1100 | 0.0710 | +0.0062 -0.0072 | +0.0113 -0.0090 | 0.0663 | +0.0061 -0.0070 | +0.0030 -0.0030 |
| 1200 | 0.0427 | +0.0039 -0.0045 | +0.0076 -0.0059 | 0.0393 | +0.0038 -0.0043 | +0.0020 -0.0020 |
| 1300 | 0.0261 | +0.0025 -0.0028 | +0.0052 -0.0040 | 0.0236 | +0.0023 -0.0026 | +0.0013 -0.0013 |
| 1400 | 0.0162 | +0.0016 -0.0018 | +0.0036 -0.0027 | 0.0144 | +0.0015 -0.0017 | +0.0009 -0.0009 |
| 1500 | 0.0102 | +0.0010 -0.0012 | +0.0026 -0.0018 | 0.0088 | +0.0010 -0.0011 | +0.0006 -0.0006 |
| 1600 | 0.0064 | +0.0007 -0.0008 | +0.0018 -0.0013 | 0.0055 | +0.0006 -0.0007 | +0.0004 -0.0004 |
| 1700 | 0.00411 | +0.00045 -0.00050 | +0.00128 -0.00087 | 0.00341 | +0.00039 -0.00043 | +0.00028 -0.00027 |
| 1800 | 0.00264 | +0.00030 -0.00033 | +0.00092 -0.00060 | 0.00214 | +0.00026 -0.00027 | +0.00019 -0.00018 |
| 1900 | 0.00171 | +0.00020 -0.00022 | +0.00066 -0.00042 | 0.00134 | +0.00017 -0.00018 | +0.00013 -0.00012 |
| 2000 | 0.00111 | +0.00014 -0.00015 | +0.00048 -0.00030 | 0.00085 | +0.00011 -0.00011 | +0.00009 -0.00008 |

Table 12: Next-to-leading order cross sections for $pp \rightarrow tW'^-$ at the 7 TeV LHC.

may consequently question the validity of cross-section results obtained using CTEQ6L1 partons and involving initial state heavy quarks, particularly at high x values (applicable to high gauge boson masses). Nevertheless, we include these here given that CTEQ6L1 partons remain in use by experimental collaborations.

In general, there may be non-zero values for all relevant P_{tD} and Q_{tU} , and the total cross-section for such a model is not simply related to the sum of the cross-sections for the individual choices $P_{tD} = 1$, $Q_{tU} = 1$. This is due to the presence of partonic channels appearing in the real emission corrections at NLO, such as $gg \rightarrow tW'\bar{D}$ and $q\bar{q} \rightarrow tW'\bar{D}$ (where \bar{D} is any down-type antiquark), which involve a sum over possible decays of an off-shell intermediate antitop. However, we have explicitly checked that the contribution of such channels is numerically extremely small (due principally to the damping effect of initial state sea quark and gluon distributions at large x). A very good approximate prescription for obtaining the total cross-section for any model is then as follows.

For tW' production, let $\sigma_{tD}^{tW'}$ be the total cross-section for $P_{tD} = 1$ (all other $P_{tj} = 0$), and $g_R = 1$ in eq. (4). The total cross-section in a model with arbitrary left- and right-handed couplings g_L and g_R is then given by

$$\sigma \simeq (|g_L|^2 + |g_R|^2) \left[|P_{td}|^2 \sigma_{td}^{tW'} + |P_{ts}|^2 \sigma_{ts}^{tW'} + |P_{tb}|^2 \sigma_{tb}^{tW'} \right]. \quad (5)$$

Similarly, for tZ' production one has

$$\sigma \simeq (|g_L|^2 + |g_R|^2) \left[|Q_{tu}|^2 \sigma_{tu}^{tZ'} + |Q_{tc}|^2 \sigma_{tc}^{tZ'} \right], \quad (6)$$

where $\sigma_{tU}^{tZ'}$ is the total cross-section for tZ' production with $Q_{tU} = 1$ (all other $Q_{tj} = 0$). Note that eqs. (5) and (6) are exact at LO, and are broken at NLO only by the additional partonic subchannels described above. This happens at the sub-percent level, and is certainly within the theoretical uncertainty as described by scale and PDF variation.

| $M(W') \text{ (GeV)}$ | $\sigma_{\text{born}}^{\text{CTEQ6L1}}(tW'^- + \bar{t}W^+) \text{ (pb)}$ | $\sigma_{\text{born}}^{\text{MSTW 2008 LO}}(tW'^- + \bar{t}W^-) \text{ (pb)}$ |
|-----------------------|--|---|
| 200 | 9.2 +1.9 -1.4 +0.58 | 10.3 +2.2 -1.7 +0.70 |
| 300 | 2.63 -0.44 +0.21 | 3.01 -0.53 +0.26 |
| 400 | 0.91 -0.16 +0.09 | 1.06 -0.20 +0.11 |
| 500 | 0.35 -0.06 +0.038 | 0.42 -0.08 +0.049 |
| 600 | 0.151 -0.028 +0.018 | 0.183 -0.036 +0.024 |
| 700 | 0.068 -0.013 +0.009 | 0.085 -0.017 +0.012 |
| 800 | 0.033 -0.006 +0.0044 | 0.041 -0.009 +0.0062 |
| 900 | 0.0162 -0.0032 +0.0023 | 0.0209 -0.0044 +0.0033 |
| 1000 | 0.0083 -0.0017 +0.0012 | 0.0109 -0.0024 +0.0018 |
| 1100 | 0.0044 -0.0009 +0.0007 | 0.0059 -0.0013 +0.0010 |
| 1200 | 0.0023 -0.0005 +0.00037 | 0.0032 -0.0007 +0.00059 |
| 1300 | 0.00128 -0.00027 +0.00021 | 0.00180 -0.00041 +0.00034 |
| 1400 | 0.00071 -0.00015 +0.00012 | 0.00103 -0.00024 +0.00020 |
| 1500 | 0.00040 -0.00009 +0.00007 | 0.00059 -0.00014 +0.00012 |
| 1600 | 0.00023 -0.00005 +0.000039 | 0.00035 -0.00008 +0.000071 |
| 1700 | 0.000129 -0.000028 +0.000023 | 0.000203 -0.000049 +0.000043 |
| 1800 | 0.000074 -0.000016 +0.000013 | 0.000120 -0.000029 +0.000026 |
| 1900 | 0.000043 -0.000010 +0.000008 | 0.000072 -0.000018 +0.000016 |
| 2000 | 0.000025 -0.000006 | 0.000043 -0.000011 |

Table 13: The sum of the leading order cross sections for $pp \rightarrow tW'^-$ and $pp \rightarrow \bar{t}W^+$ at the 7 TeV LHC. Where W' couples to ts .

| $M(W')$ (GeV) | $\sigma_{\text{nlo}}^{\text{CT10}}(tW'^- + \bar{t}W'^+) \text{ (pb)}$ | | | $\sigma_{\text{nlo}}^{\text{MSTW 2008 NLO}}(tW'^- + \bar{t}W'^+) \text{ (pb)}$ | | |
|---------------|---|------------------------|------------------------|--|------------------------|------------------------|
| 200 | 13.8 | +0.9 -1.0 | +3.1 -1.8 | 14.4 | +0.9 -1.0 | +0.9 -0.8 |
| 300 | 3.99 | +0.25 -0.29 | +0.99 -0.60 | 4.22 | +0.27 -0.31 | +0.30 -0.28 |
| 400 | 1.40 | +0.09 -0.11 | +0.38 -0.24 | 1.49 | +0.10 -0.12 | +0.12 -0.12 |
| 500 | 0.55 | +0.04 -0.04 | +0.17 -0.11 | 0.60 | +0.04 -0.05 | +0.05 -0.05 |
| 600 | 0.240 | +0.017 -0.020 | +0.081 -0.052 | 0.259 | +0.019 -0.022 | +0.026 -0.026 |
| 700 | 0.111 | +0.008 -0.010 | +0.042 -0.027 | 0.120 | +0.009 -0.011 | +0.014 -0.013 |
| 800 | 0.054 | +0.004 -0.005 | +0.023 -0.015 | 0.058 | +0.005 -0.006 | +0.007 -0.007 |
| 900 | 0.0276 | +0.0022 -0.0026 | +0.0129 -0.0081 | 0.0293 | +0.0025 -0.0029 | +0.0041 -0.0038 |
| 1000 | 0.0145 | +0.0012 -0.0014 | +0.0076 -0.0046 | 0.0153 | +0.0014 -0.0016 | +0.0023 -0.0021 |
| 1100 | 0.0079 | +0.0007 -0.0008 | +0.0047 -0.0027 | 0.0081 | +0.0008 -0.0009 | +0.0014 -0.0012 |
| 1200 | 0.0044 | +0.0004 -0.0005 | +0.0029 -0.0016 | 0.0044 | +0.0004 -0.0005 | +0.0008 -0.0007 |
| 1300 | 0.00247 | +0.00024 -0.00027 | +0.00184 -0.00101 | 0.00245 | +0.00025 -0.00028 | +0.00049 -0.00041 |
| 1400 | 0.00142 | +0.00014 -0.00016 | +0.00119 -0.00062 | 0.00138 | +0.00014 -0.00016 | +0.00030 -0.00024 |
| 1500 | 0.00083 | +0.00009 -0.00010 | +0.00078 -0.00039 | 0.00078 | +0.00009 -0.00009 | +0.00019 -0.00015 |
| 1600 | 0.00049 | +0.00005 -0.00006 | +0.00052 -0.00025 | 0.00045 | +0.00005 -0.00006 | +0.00012 -0.00009 |
| 1700 | 0.000293 | +0.000033 -0.000035 | +0.000352 -0.000158 | 0.000259 | +0.000030 -0.000033 | +0.000073 -0.000053 |
| 1800 | 0.000177 | +0.000020 -0.000022 | +0.000240 -0.000102 | 0.000150 | +0.000018 -0.000019 | +0.000046 -0.000032 |
| 1900 | 0.000107 | +0.000013 -0.000014 | +0.000165 -0.000066 | 0.000088 | +0.000011 -0.000012 | +0.000029 -0.000020 |
| 2000 | 0.000066 | +0.000008 -0.000009 | +0.000114 -0.000043 | 0.000051 | +0.000007 -0.000007 | +0.000018 -0.000012 |

Table 14: The sum of the next-to-leading order cross sections for $pp \rightarrow tW'^-$ and $pp \rightarrow \bar{t}W'^+$ at the 7 TeV LHC. Where W' couples to ts .

| $M(W') \text{ (GeV)}$ | $\sigma_{\text{born}}^{\text{CTEQ6L1}}(tW'^- + \bar{t}W^+) \text{ (pb)}$ | $\sigma_{\text{born}}^{\text{MSTW 2008 LO}}(tW'^- + \bar{t}W^+) \text{ (pb)}$ |
|-----------------------|--|---|
| 200 | 3.22 +0.37 -0.33 +0.11 | 4.08 +0.51 -0.47 +0.17 |
| 300 | 0.88 -0.10 +0.042 | 1.17 -0.15 +0.068 |
| 400 | 0.293 -0.037 +0.017 | 0.406 -0.057 +0.029 |
| 500 | 0.110 -0.015 +0.008 | 0.159 -0.024 +0.013 |
| 600 | 0.0451 -0.006 +0.0035 | 0.068 -0.011 +0.0065 |
| 700 | 0.0198 -0.0029 +0.0017 | 0.0310 -0.0052 +0.0033 |
| 800 | 0.0092 -0.0014 +0.0009 | 0.0149 -0.0026 +0.0017 |
| 900 | 0.0044 -0.0007 +0.00044 | 0.0075 -0.0014 +0.00094 |
| 1000 | 0.00221 -0.00035 +0.00023 | 0.00386 -0.00072 +0.00052 |
| 1100 | 0.00113 -0.00018 +0.00013 | 0.00205 -0.00039 +0.00029 |
| 1200 | 0.00060 -0.00010 +0.00007 | 0.00112 -0.00022 +0.00017 |
| 1300 | 0.00032 -0.00005 +0.000038 | 0.00062 -0.00012 +0.000097 |
| 1400 | 0.000174 -0.000030 +0.000021 | 0.000348 -0.000072 +0.000057 |
| 1500 | 0.000096 -0.000017 +0.000012 | 0.000198 -0.000042 +0.000034 |
| 1600 | 0.000054 -0.000010 +0.000007 | 0.000114 -0.000025 +0.000020 |
| 1700 | 0.000031 -0.000005 +0.0000041 | 0.000066 -0.000015 +0.0000121 |
| 1800 | 0.0000174 -0.0000031 +0.0000024 | 0.0000389 -0.0000087 +0.0000073 |
| 1900 | 0.0000100 -0.0000018 +0.0000014 | 0.0000229 -0.0000052 +0.0000044 |
| 2000 | 0.0000058 -0.0000011 | 0.0000136 -0.0000031 |

Table 15: The sum of the leading order cross sections for $pp \rightarrow tW'^-$ and $pp \rightarrow \bar{t}W^+$ at the 7 TeV LHC. Where W' couples to tb .

| $M(W')$ (GeV) | $\sigma_{\text{nlo}}^{\text{CT10}}(tW'^- + \bar{t}W'^+) \text{ (pb)}$ | | | $\sigma_{\text{nlo}}^{\text{MSTW 2008 NLO}}(tW'^- + \bar{t}W'^+) \text{ (pb)}$ | | |
|---------------|---|------------|------------|--|------------|------------|
| 200 | 4.61 | +0.29 | +0.57 | 4.98 | +0.32 | +0.22 |
| | | -0.25 | -0.49 | | -0.27 | -0.29 |
| 300 | 1.30 | +0.08 | +0.21 | 1.40 | +0.08 | +0.08 |
| | | -0.06 | -0.18 | | -0.06 | -0.10 |
| 400 | 0.452 | +0.024 | +0.089 | 0.480 | +0.026 | +0.032 |
| | | -0.019 | -0.074 | | -0.021 | -0.039 |
| 500 | 0.178 | +0.009 | +0.042 | 0.187 | +0.010 | +0.015 |
| | | -0.008 | -0.034 | | -0.009 | -0.017 |
| 600 | 0.077 | +0.004 | +0.022 | 0.078 | +0.004 | +0.007 |
| | | -0.004 | -0.017 | | -0.004 | -0.008 |
| 700 | 0.0355 | +0.0016 | +0.0118 | 0.0363 | +0.0018 | +0.0037 |
| | | -0.0019 | -0.0087 | | -0.0021 | -0.0041 |
| 800 | 0.0173 | +0.0008 | +0.0066 | 0.0174 | +0.0009 | +0.0020 |
| | | -0.0010 | -0.0047 | | -0.0011 | -0.0022 |
| 900 | 0.0088 | +0.0004 | +0.0039 | 0.0087 | +0.0005 | +0.0011 |
| | | -0.0005 | -0.0026 | | -0.0006 | -0.0012 |
| 1000 | 0.00464 | +0.00025 | +0.00233 | 0.00448 | +0.00026 | +0.00062 |
| | | -0.00030 | -0.00151 | | -0.00031 | -0.00066 |
| 1100 | 0.00252 | +0.00014 | +0.00143 | 0.00238 | +0.00014 | +0.00036 |
| | | -0.00017 | -0.00089 | | -0.00017 | -0.00038 |
| 1200 | 0.00140 | +0.00008 | +0.00090 | 0.00129 | +0.00008 | +0.00021 |
| | | -0.00010 | -0.00053 | | -0.00010 | -0.00022 |
| 1300 | 0.00079 | +0.00005 | +0.00057 | 0.00071 | +0.00005 | +0.00013 |
| | | -0.00006 | -0.00033 | | -0.00006 | -0.00013 |
| 1400 | 0.000458 | +0.000030 | +0.000369 | 0.000400 | +0.000028 | +0.000075 |
| | | -0.000036 | -0.000204 | | -0.000034 | -0.000077 |
| 1500 | 0.000269 | +0.000018 | +0.000242 | 0.000227 | +0.000017 | +0.000046 |
| | | -0.000022 | -0.000128 | | -0.000020 | -0.000046 |
| 1600 | 0.000159 | +0.000011 | +0.000160 | 0.000131 | +0.000010 | +0.000028 |
| | | -0.000014 | -0.000081 | | -0.000012 | -0.000028 |
| 1700 | 0.000096 | +0.000007 | +0.000107 | 0.000076 | +0.000006 | +0.000017 |
| | | -0.000009 | -0.000052 | | -0.000007 | -0.000017 |
| 1800 | 0.000058 | +0.000005 | +0.000072 | 0.000044 | +0.000004 | +0.000011 |
| | | -0.000006 | -0.000034 | | -0.000004 | -0.000011 |
| 1900 | 0.0000352 | +0.0000029 | +0.0000485 | 0.0000260 | +0.0000023 | +0.0000067 |
| | | -0.0000035 | -0.0000219 | | -0.0000026 | -0.0000065 |
| 2000 | 0.0000215 | +0.0000019 | +0.0000330 | 0.0000153 | +0.0000014 | +0.0000042 |
| | | -0.0000022 | -0.0000142 | | -0.0000016 | -0.0000040 |

Table 16: The sum of the next-to-leading order cross sections for $pp \rightarrow tW'^-$ and $pp \rightarrow \bar{t}W'^+$ at the 7 TeV LHC. Where W' couples to tb .

| $M(Z') \text{ (GeV)}$ | $\sigma_{\text{born}}^{\text{CTEQ6L1}}(tZ' + \bar{t}Z') \text{ (pb)}$ | $\sigma_{\text{born}}^{\text{MSTW 2008 LO}}(tZ' + \bar{t}Z') \text{ (pb)}$ |
|-----------------------|---|--|
| 200 | 5.31 +0.91 -0.74 +0.27 | 6.89 +1.26 -1.02 +0.41 |
| 300 | 1.46 -0.22 +0.10 -0.08 | 2.00 -0.32 +0.16 -0.12 |
| 400 | 0.49 +0.039 -0.030 +0.017 | 0.70 +0.065 -0.050 +0.030 |
| 500 | 0.183 -0.013 +0.008 -0.006 | 0.279 -0.022 +0.014 -0.011 |
| 600 | 0.075 +0.0036 -0.0027 +0.0018 | 0.121 +0.0073 -0.0054 +0.0038 |
| 700 | 0.0331 -0.0013 +0.0009 -0.0007 | 0.056 -0.0015 +0.0021 -0.0015 |
| 800 | 0.0154 +0.0005 -0.0004 -0.00019 | 0.0273 +0.0012 -0.0008 +0.00065 |
| 900 | 0.0074 +0.00026 -0.00019 +0.00014 | 0.0139 +0.00031 -0.00029 +0.00019 |
| 1000 | 0.0037 -0.00010 +0.00008 -0.00006 | 0.0073 -0.00018 +0.00012 -0.00011 |
| 1100 | 0.0019 +0.00008 -0.00006 +0.000043 | 0.0039 +0.00022 -0.00016 +0.000130 |
| 1200 | 0.00101 +0.000025 -0.000032 +0.000025 | 0.00216 +0.000078 -0.000091 +0.000078 |
| 1300 | 0.00054 -0.000018 +0.000014 -0.000010 | 0.00121 -0.000042 +0.000047 -0.000032 |
| 1400 | 0.00030 +0.000008 -0.000006 +0.0000047 | 0.00069 +0.000028 -0.000020 +0.0000173 |
| 1500 | 0.000163 -0.0000034 +0.0000027 -0.0000020 | 0.000400 -0.0000119 +0.0000106 -0.0000072 |
| 1600 | 0.000091 +0.0000027 -0.0000020 | 0.000234 +0.0000077 -0.0000067 |
| 1700 | 0.000052 +0.0000014 -0.0000010 +0.0000008 | 0.000138 +0.0000047 -0.0000032 +0.0000028 |
| 1800 | 0.000030 -0.0000006 +0.00000047 -0.00000034 | 0.000082 -0.0000017 +0.00000121 -0.0000106 |
| 1900 | 0.0000169 +0.00000047 -0.00000034 +0.00000027 | 0.0000490 +0.00000173 -0.00000119 +0.00000106 |
| 2000 | 0.0000098 -0.00000020 | 0.0000294 -0.0000072 |

Table 17: The sum of the leading order cross sections for $pp \rightarrow \bar{t}Z'$ and $pp \rightarrow tZ'$ at the 7 TeV LHC. Where Z' couples to tc .

| $M(Z') \text{ (GeV)}$ | $\sigma_{\text{nlo}}^{\text{CT10}}(tZ' + \bar{t}Z') \text{ (pb)}$ | | | $\sigma_{\text{nlo}}^{\text{MSTW 2008 NLO}}(tZ' + \bar{t}Z') \text{ (pb)}$ | | |
|-----------------------|---|--------------------------|--------------------------|--|--------------------------|--------------------------|
| 200 | 7.92 | +0.44 -0.45 | +0.98 -0.86 | 8.41 | +0.49 -0.50 | +0.40 -0.51 |
| 300 | 2.26 | +0.12 -0.13 | +0.36 -0.31 | 2.38 | +0.13 -0.15 | +0.14 -0.17 |
| 400 | 0.78 | +0.04 -0.05 | +0.16 -0.13 | 0.82 | +0.05 -0.05 | +0.06 -0.07 |
| 500 | 0.310 | +0.018 -0.021 | +0.075 -0.062 | 0.321 | +0.019 -0.023 | +0.026 -0.031 |
| 600 | 0.134 | +0.008 -0.009 | +0.039 -0.031 | 0.137 | +0.009 -0.010 | +0.013 -0.015 |
| 700 | 0.062 | +0.004 -0.005 | +0.021 -0.016 | 0.063 | +0.004 -0.005 | +0.007 -0.008 |
| 800 | 0.0306 | +0.0020 -0.0024 | +0.0120 -0.0087 | 0.0303 | +0.0021 -0.0025 | +0.0036 -0.0041 |
| 900 | 0.0157 | +0.0011 -0.0013 | +0.0071 -0.0049 | 0.0152 | +0.0011 -0.0013 | +0.0020 -0.0022 |
| 1000 | 0.0083 | +0.0006 -0.0007 | +0.0043 -0.0029 | 0.0079 | +0.0006 -0.0007 | +0.0012 -0.0013 |
| 1100 | 0.00454 | +0.00034 -0.00040 | +0.00266 -0.00169 | 0.00422 | +0.00034 -0.00039 | +0.00067 -0.00072 |
| 1200 | 0.00254 | +0.00020 -0.00023 | +0.00168 -0.00103 | 0.00230 | +0.00019 -0.00022 | +0.00040 -0.00042 |
| 1300 | 0.00145 | +0.00012 -0.00014 | +0.00108 -0.00063 | 0.00128 | +0.00011 -0.00013 | +0.00024 -0.00025 |
| 1400 | 0.00085 | +0.00007 -0.00008 | +0.00070 -0.00040 | 0.00072 | +0.00007 -0.00007 | +0.00015 -0.00015 |
| 1500 | 0.00050 | +0.00005 -0.00005 | +0.00046 -0.00025 | 0.00041 | +0.00004 -0.00004 | +0.00009 -0.00009 |
| 1600 | 0.000298 | +0.000028 -0.000032 | +0.000308 -0.000161 | 0.000239 | +0.000024 -0.000026 | +0.000055 -0.000056 |
| 1700 | 0.000180 | +0.000018 -0.000020 | +0.000207 -0.000104 | 0.000139 | +0.000014 -0.000016 | +0.000034 -0.000034 |
| 1800 | 0.000110 | +0.000011 -0.000012 | +0.000140 -0.000067 | 0.000082 | +0.000009 -0.000010 | +0.000021 -0.000021 |
| 1900 | 0.000068 | +0.000007 -0.000008 | +0.000096 -0.000044 | 0.000048 | +0.000005 -0.000006 | +0.000013 -0.000013 |
| 2000 | 0.0000417 | +0.0000046 -0.0000050 | +0.0000657 -0.0000290 | 0.0000287 | +0.0000033 -0.0000035 | +0.0000084 -0.0000081 |

Table 18: The sum of the next-to-leading order cross sections for $pp \rightarrow \bar{t}Z'$ and $pp \rightarrow tZ'$ at the 7 TeV LHC. Where Z' couples to tc .

| $M(Z') \text{ (GeV)}$ | $\sigma_{\text{born}}^{\text{CTEQ6L1}}(tZ' + \bar{t}Z') \text{ (pb)}$ | $\sigma_{\text{born}}^{\text{MSTW 2008 LO}}(tZ' + \bar{t}Z') \text{ (pb)}$ |
|-----------------------|---|--|
| 200 | 104.7 +20.7 -16.1 | 106.2 +22.0 -17.0 |
| 300 | 36.98 +7.80 -5.99 | 37.66 +8.33 -6.33 |
| 400 | 15.47 +3.43 -2.61 | 15.84 +3.68 -2.77 |
| 500 | 7.218 +1.662 -1.254 | 7.440 +1.804 -1.346 |
| 600 | 3.637 +0.864 -0.648 | 3.775 +0.949 -0.703 |
| 700 | 1.941 +0.474 -0.354 | 2.030 +0.526 -0.388 |
| 800 | 1.083 +0.271 -0.201 | 1.142 +0.304 -0.223 |
| 900 | 0.626 +0.160 -0.118 | 0.665 +0.182 -0.133 |
| 1000 | 0.373 +0.097 -0.071 | 0.399 +0.112 -0.081 |
| 1100 | 0.227 +0.060 -0.044 | 0.245 +0.070 -0.051 |
| 1200 | 0.141 +0.038 -0.028 | 0.153 +0.045 -0.032 |
| 1300 | 0.0891 +0.0243 -0.0178 | 0.0976 +0.0292 -0.0208 |
| 1400 | 0.0571 +0.0158 -0.0115 | 0.0630 +0.0192 -0.0136 |
| 1500 | 0.0370 +0.0104 -0.0075 | 0.0411 +0.0128 -0.0090 |
| 1600 | 0.0242 +0.0069 -0.0050 | 0.0271 +0.0086 -0.0060 |
| 1700 | 0.0160 +0.0046 -0.0033 | 0.0180 +0.0058 -0.0041 |
| 1800 | 0.0107 +0.0031 -0.0022 | 0.0121 +0.0039 -0.0028 |
| 1900 | 0.00714 +0.00210 -0.00151 | 0.00813 +0.00270 -0.00188 |
| 2000 | 0.00480 +0.00143 -0.00102 | 0.00550 +0.00186 -0.00129 |

Table 19: The sum of the leading order cross sections for $pp \rightarrow \bar{t}Z'$ and $pp \rightarrow tZ'$ at the 8 TeV LHC.

A.3 Cross-section results at 8 TeV

In this section, we present cross-section results at the LHC, for a centre of mass energy of 8 TeV. These can then be directly applied to current ATLAS and CMS analyses, as in the case of the 7 TeV results.

Total LO cross-sections for top or anti-top production in association with a Z' boson can be found in table 19. Individual results for t or \bar{t} production are in tables 20 and 21. The corresponding LO results for W' production can be found in tables 22-24, and NLO results for all the above in tables 25-30.

For completeness, we also present results for different choices of the partonic couplings P_{tD} and Q_{tU} (similarly to appendix A.2), in tables 31-36. These results can be combined to yield (very good) approximate cross-sections for any model encapsulated by eq. (4), according to the prescription of eqs. (5) and (6).

| $M(Z') \text{ (GeV)}$ | $\sigma_{\text{born}}^{\text{CTEQ6L1}}(\bar{t}Z') \text{ (pb)}$ | $\sigma_{\text{born}}^{\text{MSTW 2008 LO}}(\bar{t}Z') \text{ (pb)}$ |
|-----------------------|---|--|
| 200 | 9.5 +2.0 -1.5 | 11.6 +2.5 -1.9 |
| 300 | 2.89 +0.64 -0.48 | 3.61 +0.84 -0.63 |
| 400 | 1.05 +0.24 -0.18 | 1.35 +0.33 -0.25 |
| 500 | 0.433 +0.104 -0.078 | 0.569 +0.146 -0.108 |
| 600 | 0.194 +0.048 -0.036 | 0.261 +0.069 -0.051 |
| 700 | 0.093 +0.024 -0.018 | 0.128 +0.035 -0.025 |
| 800 | 0.047 +0.012 -0.009 | 0.066 +0.019 -0.013 |
| 900 | 0.0245 +0.0065 -0.0048 | 0.0350 +0.0102 -0.0073 |
| 1000 | 0.0133 +0.0036 -0.0026 | 0.0193 +0.0058 -0.0041 |
| 1100 | 0.0074 +0.0020 -0.0015 | 0.0109 +0.0033 -0.0024 |
| 1200 | 0.0042 +0.0012 -0.0009 | 0.0063 +0.0020 -0.0014 |
| 1300 | 0.0025 +0.0007 -0.0005 | 0.0037 +0.0012 -0.0008 |
| 1400 | 0.00145 +0.00041 -0.00030 | 0.00224 +0.00073 -0.00051 |
| 1500 | 0.00087 +0.00025 -0.00018 | 0.00136 +0.00045 -0.00031 |
| 1600 | 0.00053 +0.00015 -0.00011 | 0.00083 +0.00028 -0.00019 |
| 1700 | 0.00032 +0.00010 -0.00007 | 0.00052 +0.00018 -0.00012 |
| 1800 | 0.00020 +0.00006 -0.00004 | 0.00032 +0.00011 -0.00008 |
| 1900 | 0.000124 +0.000038 -0.000027 | 0.000202 +0.000072 -0.000049 |
| 2000 | 0.000077 +0.000024 -0.000017 | 0.000128 +0.000046 -0.000031 |

Table 20: Leading order cross sections for $pp \rightarrow \bar{t}Z'$ at the 8 TeV LHC.

| $M(Z')$ (GeV) | $\sigma_{\text{born}}^{\text{CTEQ6L1}}(tZ')$ (pb) | $\sigma_{\text{born}}^{\text{MSTW 2008 LO}}(tZ')$ (pb) |
|---------------|---|--|
| 200 | 95.2 +18.8 -14.6 | 94.6 +19.5 -15.1 |
| 300 | 34.1 +7.2 -5.5 | 34.1 +7.5 -5.7 |
| 400 | 14.42 +3.18 -2.42 | 14.49 +3.35 -2.53 |
| 500 | 6.79 +1.56 -1.18 | 6.87 +1.66 -1.24 |
| 600 | 3.44 +0.82 -0.61 | 3.52 +0.88 -0.65 |
| 700 | 1.848 +0.450 -0.336 | 1.903 +0.491 -0.362 |
| 800 | 1.036 +0.259 -0.192 | 1.076 +0.286 -0.209 |
| 900 | 0.602 +0.153 -0.113 | 0.630 +0.172 -0.125 |
| 1000 | 0.359 +0.093 -0.069 | 0.380 +0.106 -0.077 |
| 1100 | 0.220 +0.058 -0.043 | 0.234 +0.067 -0.048 |
| 1200 | 0.137 +0.037 -0.027 | 0.147 +0.043 -0.031 |
| 1300 | 0.0867 +0.0237 -0.0173 | 0.0939 +0.0280 -0.0200 |
| 1400 | 0.0556 +0.0154 -0.0112 | 0.0607 +0.0185 -0.0131 |
| 1500 | 0.0362 +0.0101 -0.0074 | 0.0398 +0.0123 -0.0087 |
| 1600 | 0.0237 +0.0067 -0.0049 | 0.0263 +0.0083 -0.0058 |
| 1700 | 0.0157 +0.0045 -0.0033 | 0.0175 +0.0056 -0.0039 |
| 1800 | 0.0105 +0.0030 -0.0022 | 0.0117 +0.0038 -0.0027 |
| 1900 | 0.0070 +0.0021 -0.0015 | 0.0079 +0.0026 -0.0018 |
| 2000 | 0.00473 +0.00140 -0.00101 | 0.00537 +0.00181 -0.00126 |

Table 21: Leading order cross sections for $pp \rightarrow tZ'$ at the 8 TeV LHC.

| $M(W')$ (GeV) | $\sigma_{\text{born}}^{\text{CTEQ6L1}}(tW'^- + \bar{t}W'^+) \text{ (pb)}$ | $\sigma_{\text{born}}^{\text{MSTW 2008 LO}}(tW'^- + \bar{t}W'^+) \text{ (pb)}$ |
|---------------|---|--|
| 200 | 57.7 +11.9 -9.2 +4.27 | 58.7 +12.8 -9.8 +4.60 |
| 300 | 19.43 -3.25 +1.79 | 19.81 -3.46 +1.94 |
| 400 | 7.79 -1.35 +0.84 | 7.96 -1.45 +0.91 |
| 500 | 3.49 -0.62 +0.418 | 3.58 -0.67 +0.460 |
| 600 | 1.692 -0.310 +0.221 | 1.743 -0.337 +0.245 |
| 700 | 0.871 -0.163 +0.122 | 0.902 -0.179 +0.137 |
| 800 | 0.470 -0.090 +0.069 | 0.488 -0.099 +0.079 |
| 900 | 0.263 -0.051 +0.041 | 0.274 -0.057 +0.047 |
| 1000 | 0.151 -0.030 +0.0245 | 0.159 -0.033 +0.0283 |
| 1100 | 0.0895 -0.0178 +0.0150 | 0.0941 -0.0201 +0.0175 |
| 1200 | 0.0539 -0.0109 +0.0093 | 0.0570 -0.0124 +0.0110 |
| 1300 | 0.0331 -0.0067 +0.0059 | 0.0351 -0.0077 +0.0070 |
| 1400 | 0.0206 -0.0042 +0.0037 | 0.0219 -0.0049 +0.0045 |
| 1500 | 0.0130 -0.0027 +0.0024 | 0.0138 -0.0031 +0.0029 |
| 1600 | 0.0083 -0.0017 +0.00157 | 0.0088 -0.0020 +0.00191 |
| 1700 | 0.00529 -0.00112 +0.00102 | 0.00568 -0.00132 +0.00126 |
| 1800 | 0.00342 -0.00073 +0.00067 | 0.00368 -0.00087 +0.00083 |
| 1900 | 0.00223 -0.00048 +0.00045 | 0.00240 -0.00057 +0.00056 |
| 2000 | 0.00146 -0.00032 | 0.00158 -0.00038 |

Table 22: The sum of the leading order cross sections for $pp \rightarrow tW'^-$ and $pp \rightarrow \bar{t}W'^+$ at the 8 TeV LHC.

| $M(W'^+) \text{ (GeV)}$ | $\sigma_{\text{born}}^{\text{CTEQ6L1}}(\bar{t}W'^+) \text{ (pb)}$ | | $\sigma_{\text{born}}^{\text{MSTW 2008 LO}}(\bar{t}W'^+) \text{ (pb)}$ | |
|-------------------------|---|--------------------------|--|------------------------|
| 200 | 12.2 | +2.6 -2.0 | 13.7 | +3.1 -2.3 |
| 300 | 3.76 | +0.85 -0.64 | 4.30 | +1.03 -0.77 |
| 400 | 1.39 | +0.33 -0.25 | 1.61 | +0.41 -0.30 |
| 500 | 0.575 | +0.142 -0.106 | 0.674 | +0.179 -0.131 |
| 600 | 0.259 | +0.066 -0.049 | 0.306 | +0.084 -0.061 |
| 700 | 0.124 | +0.033 -0.024 | 0.148 | +0.042 -0.030 |
| 800 | 0.062 | +0.017 -0.012 | 0.075 | +0.022 -0.016 |
| 900 | 0.0325 | +0.0089 -0.0065 | 0.0392 | +0.0118 -0.0084 |
| 1000 | 0.0175 | +0.0049 -0.0035 | 0.0212 | +0.0066 -0.0046 |
| 1100 | 0.0096 | +0.0027 -0.0020 | 0.0117 | +0.0037 -0.0026 |
| 1200 | 0.0054 | +0.0016 -0.0011 | 0.0066 | +0.0021 -0.0015 |
| 1300 | 0.00310 | +0.00091 -0.00065 | 0.00379 | +0.00125 -0.00087 |
| 1400 | 0.00180 | +0.00053 -0.00038 | 0.00220 | +0.00074 -0.00051 |
| 1500 | 0.00106 | +0.00032 -0.00023 | 0.00129 | +0.00044 -0.00031 |
| 1600 | 0.00063 | +0.00019 -0.00014 | 0.00077 | +0.00027 -0.00019 |
| 1700 | 0.00037 | +0.00012 -0.00008 | 0.00046 | +0.00016 -0.00011 |
| 1800 | 0.00023 | +0.00007 -0.00005 | 0.00028 | +0.00010 -0.00007 |
| 1900 | 0.000136 | +0.000043 -0.000030 | 0.000169 | +0.000062 -0.000042 |
| 2000 | 0.0000828 | +0.0000262 -0.0000185 | 0.000103 | +0.000038 -0.000026 |

Table 23: Leading order cross sections for $pp \rightarrow \bar{t}W'^+$ at the 8 TeV LHC.

| $M(W'^-) \text{ (GeV)}$ | $\sigma_{\text{born}}^{\text{CTEQ6L1}}(tW'^-) \text{ (pb)}$ | $\sigma_{\text{born}}^{\text{MSTW 2008 LO}}(tW'^-) \text{ (pb)}$ |
|-------------------------|---|--|
| 200 | 45.5 +9.3 -7.2 | 45.0 +9.7 -7.4 |
| 300 | 15.68 +3.42 -2.61 | 15.51 +3.57 -2.69 |
| 400 | 6.40 +1.47 -1.11 | 6.35 +1.54 -1.15 |
| 500 | 2.91 +0.69 -0.52 | 2.91 +0.73 -0.54 |
| 600 | 1.433 +0.352 -0.262 | 1.437 +0.375 -0.276 |
| 700 | 0.747 +0.188 -0.139 | 0.754 +0.203 -0.148 |
| 800 | 0.407 +0.105 -0.077 | 0.414 +0.115 -0.083 |
| 900 | 0.230 +0.061 -0.044 | 0.235 +0.067 -0.048 |
| 1000 | 0.134 +0.036 -0.026 | 0.138 +0.040 -0.029 |
| 1100 | 0.0798 +0.0218 -0.0159 | 0.0824 +0.0246 -0.0175 |
| 1200 | 0.0485 +0.0134 -0.0098 | 0.0504 +0.0153 -0.0109 |
| 1300 | 0.0300 +0.0084 -0.0061 | 0.0313 +0.0097 -0.0069 |
| 1400 | 0.0188 +0.0053 -0.0039 | 0.0197 +0.0062 -0.0044 |
| 1500 | 0.0119 +0.0034 -0.0025 | 0.0125 +0.0040 -0.0028 |
| 1600 | 0.0076 +0.0022 -0.0016 | 0.0081 +0.0027 -0.0019 |
| 1700 | 0.00492 +0.00145 -0.00104 | 0.00522 +0.00175 -0.00121 |
| 1800 | 0.00320 +0.00096 -0.00068 | 0.00341 +0.00116 -0.00080 |
| 1900 | 0.00209 +0.00063 -0.00045 | 0.00223 +0.00077 -0.00053 |
| 2000 | 0.00137 +0.00042 -0.00030 | 0.00147 +0.00052 -0.00035 |

Table 24: Leading order cross sections for $pp \rightarrow tW'^-$ at the 8 TeV LHC.

| $M(Z')$ (GeV) | $\sigma_{\text{nlo}}^{\text{CT10}}(tZ' + \bar{t}Z')$ (pb) | | | $\sigma_{\text{nlo}}^{\text{MSTW 2008 NLO}}(tZ' + \bar{t}Z')$ (pb) | | |
|---------------|---|--------------------|--------------------|--|--------------------|--------------------|
| 200 | 134.7 | +8.8 -9.1 | +3.2 -3.6 | 137.7 | +9.2 -9.6 | +1.3 -0.9 |
| 300 | 48.43 | +3.08 -3.40 | +1.31 -1.39 | 49.48 | +3.25 -3.55 | +0.48 -0.32 |
| 400 | 20.63 | +1.32 -1.50 | +0.69 -0.67 | 21.07 | +1.39 -1.57 | +0.23 -0.16 |
| 500 | 9.80 | +0.64 -0.75 | +0.40 -0.37 | 10.00 | +0.67 -0.78 | +0.13 -0.10 |
| 600 | 5.03 | +0.34 -0.40 | +0.24 -0.22 | 5.12 | +0.35 -0.41 | +0.08 -0.06 |
| 700 | 2.73 | +0.19 -0.22 | +0.16 -0.14 | 2.78 | +0.20 -0.23 | +0.05 -0.04 |
| 800 | 1.549 | +0.111 -0.131 | +0.104 -0.091 | 1.573 | +0.116 -0.135 | +0.033 -0.028 |
| 900 | 0.911 | +0.067 -0.080 | +0.070 -0.061 | 0.923 | +0.070 -0.082 | +0.022 -0.019 |
| 1000 | 0.552 | +0.042 -0.050 | +0.048 -0.041 | 0.557 | +0.044 -0.051 | +0.015 -0.013 |
| 1100 | 0.342 | +0.027 -0.032 | +0.034 -0.029 | 0.344 | +0.028 -0.032 | +0.011 -0.009 |
| 1200 | 0.217 | +0.018 -0.021 | +0.024 -0.020 | 0.217 | +0.018 -0.021 | +0.007 -0.007 |
| 1300 | 0.139 | +0.012 -0.014 | +0.017 -0.014 | 0.139 | +0.012 -0.014 | +0.005 -0.005 |
| 1400 | 0.0910 | +0.0079 -0.0092 | +0.0127 -0.0101 | 0.0901 | +0.0081 -0.0092 | +0.0037 -0.0035 |
| 1500 | 0.0601 | +0.0054 -0.0062 | +0.0094 -0.0072 | 0.0591 | +0.0055 -0.0062 | +0.0027 -0.0025 |
| 1600 | 0.0401 | +0.0037 -0.0043 | +0.0070 -0.0052 | 0.0392 | +0.0038 -0.0042 | +0.0019 -0.0018 |
| 1700 | 0.0270 | +0.0026 -0.0029 | +0.0052 -0.0037 | 0.0262 | +0.0026 -0.0029 | +0.0014 -0.0013 |
| 1800 | 0.0183 | +0.0018 -0.0020 | +0.0039 -0.0027 | 0.0176 | +0.0018 -0.0020 | +0.0010 -0.0009 |
| 1900 | 0.0125 | +0.0013 -0.0014 | +0.0030 -0.0020 | 0.0119 | +0.0013 -0.0014 | +0.0007 -0.0007 |
| 2000 | 0.0086 | +0.0009 -0.0010 | +0.0023 -0.0015 | 0.0081 | +0.0009 -0.0010 | +0.0005 -0.0005 |

Table 25: The sum of the next-to-leading order cross sections for $pp \rightarrow tZ'$ and $pp \rightarrow \bar{t}Z'$ at the 8 TeV LHC.

| $M(Z') \text{ (GeV)}$ | $\sigma_{\text{nlo}}^{\text{CT10}}(\bar{t}Z') \text{ (pb)}$ | | | $\sigma_{\text{nlo}}^{\text{MSTW 2008 NLO}}(\bar{t}Z') \text{ (pb)}$ | | |
|-----------------------|---|------------------------|------------------------|--|------------------------|------------------------|
| 200 | 13.2 | +0.8 -0.9 | +1.1 -1.2 | 14.8 | +1.0 -1.1 | +0.5 -0.4 |
| 300 | 4.11 | +0.26 -0.29 | +0.39 -0.42 | 4.63 | +0.30 -0.34 | +0.17 -0.16 |
| 400 | 1.54 | +0.10 -0.12 | +0.17 -0.18 | 1.74 | +0.12 -0.14 | +0.08 -0.07 |
| 500 | 0.65 | +0.04 -0.05 | +0.09 -0.08 | 0.74 | +0.05 -0.06 | +0.04 -0.04 |
| 600 | 0.299 | +0.021 -0.025 | +0.046 -0.043 | 0.339 | +0.025 -0.029 | +0.020 -0.019 |
| 700 | 0.147 | +0.011 -0.013 | +0.026 -0.023 | 0.167 | +0.013 -0.015 | +0.011 -0.010 |
| 800 | 0.076 | +0.006 -0.007 | +0.015 -0.013 | 0.086 | +0.007 -0.008 | +0.007 -0.006 |
| 900 | 0.041 | +0.003 -0.004 | +0.009 -0.008 | 0.046 | +0.004 -0.004 | +0.004 -0.004 |
| 1000 | 0.0227 | +0.0019 -0.0022 | +0.0058 -0.0046 | 0.0257 | +0.0022 -0.0025 | +0.0024 -0.0022 |
| 1100 | 0.0130 | +0.0011 -0.0013 | +0.0037 -0.0028 | 0.0146 | +0.0013 -0.0015 | +0.0015 -0.0014 |
| 1200 | 0.0076 | +0.0007 -0.0008 | +0.0024 -0.0018 | 0.0085 | +0.0008 -0.0009 | +0.0010 -0.0009 |
| 1300 | 0.0045 | +0.0004 -0.0005 | +0.0016 -0.0012 | 0.0051 | +0.0005 -0.0005 | +0.0006 -0.0006 |
| 1400 | 0.00275 | +0.00026 -0.00029 | +0.00107 -0.00075 | 0.00305 | +0.00030 -0.00034 | +0.00040 -0.00038 |
| 1500 | 0.00169 | +0.00017 -0.00019 | +0.00073 -0.00049 | 0.00186 | +0.00019 -0.00021 | +0.00026 -0.00025 |
| 1600 | 0.00106 | +0.00011 -0.00012 | +0.00050 -0.00033 | 0.00115 | +0.00012 -0.00013 | +0.00018 -0.00016 |
| 1700 | 0.00066 | +0.00007 -0.00008 | +0.00035 -0.00022 | 0.00072 | +0.00008 -0.00009 | +0.00012 -0.00011 |
| 1800 | 0.00042 | +0.00005 -0.00005 | +0.00024 -0.00015 | 0.00045 | +0.00005 -0.00006 | +0.00008 -0.00007 |
| 1900 | 0.000270 | +0.000030 -0.000033 | +0.000169 -0.000099 | 0.000283 | +0.000033 -0.000035 | +0.000052 -0.000049 |
| 2000 | 0.000174 | +0.000020 -0.000022 | +0.000119 -0.000068 | 0.000179 | +0.000022 -0.000023 | +0.000035 -0.000033 |

Table 26: Next-to-leading order cross sections for $pp \rightarrow \bar{t}Z'$ at the 8 TeV LHC.

| $M(Z') (\text{GeV})$ | $\sigma_{\text{nlo}}^{\text{CT10}}(tZ') (\text{pb})$ | | | $\sigma_{\text{nlo}}^{\text{MSTW 2008 NLO}}(tZ') (\text{pb})$ | | |
|----------------------|--|--------------------|--------------------|---|--------------------|--------------------|
| 200 | 121.5 | +7.9 -8.2 | +3.0 -3.3 | 122.9 | +8.3 -8.5 | +1.4 -1.0 |
| 300 | 44.33 | +2.81 -3.11 | +1.21 -1.29 | 44.86 | +2.94 -3.21 | +0.50 -0.34 |
| 400 | 19.10 | +1.21 -1.39 | +0.62 -0.62 | 19.33 | +1.27 -1.44 | +0.22 -0.16 |
| 500 | 9.15 | +0.60 -0.69 | +0.36 -0.34 | 9.26 | +0.62 -0.71 | +0.12 -0.09 |
| 600 | 4.73 | +0.32 -0.37 | +0.22 -0.20 | 4.78 | +0.33 -0.38 | +0.07 -0.06 |
| 700 | 2.58 | +0.18 -0.21 | +0.14 -0.13 | 2.61 | +0.18 -0.22 | +0.04 -0.04 |
| 800 | 1.473 | +0.106 -0.124 | +0.094 -0.085 | 1.486 | +0.110 -0.128 | +0.029 -0.025 |
| 900 | 0.871 | +0.064 -0.076 | +0.064 -0.057 | 0.876 | +0.066 -0.078 | +0.020 -0.017 |
| 1000 | 0.529 | +0.040 -0.048 | +0.044 -0.039 | 0.531 | +0.042 -0.049 | +0.014 -0.012 |
| 1100 | 0.329 | +0.026 -0.030 | +0.031 -0.027 | 0.330 | +0.027 -0.031 | +0.010 -0.009 |
| 1200 | 0.209 | +0.017 -0.020 | +0.022 -0.019 | 0.208 | +0.017 -0.020 | +0.007 -0.006 |
| 1300 | 0.135 | +0.011 -0.013 | +0.016 -0.013 | 0.134 | +0.012 -0.013 | +0.005 -0.004 |
| 1400 | 0.0882 | +0.0077 -0.0089 | +0.0119 -0.0096 | 0.0870 | +0.0078 -0.0089 | +0.0035 -0.0032 |
| 1500 | 0.0584 | +0.0052 -0.0060 | +0.0088 -0.0069 | 0.0573 | +0.0053 -0.0060 | +0.0025 -0.0023 |
| 1600 | 0.0391 | +0.0036 -0.0041 | +0.0066 -0.0050 | 0.0380 | +0.0036 -0.0041 | +0.0018 -0.0017 |
| 1700 | 0.0264 | +0.0025 -0.0029 | +0.0049 -0.0036 | 0.0255 | +0.0025 -0.0028 | +0.0013 -0.0012 |
| 1800 | 0.0179 | +0.0018 -0.0020 | +0.0037 -0.0027 | 0.0172 | +0.0017 -0.0019 | +0.0010 -0.0009 |
| 1900 | 0.0123 | +0.0013 -0.0014 | +0.0028 -0.0020 | 0.0116 | +0.0012 -0.0013 | +0.0007 -0.0007 |
| 2000 | 0.0084 | +0.0009 -0.0010 | +0.0022 -0.0014 | 0.0079 | +0.0009 -0.0009 | +0.0005 -0.0005 |

Table 27: Next-to-leading order cross sections for $pp \rightarrow tZ'$ at the 8 TeV LHC.

| $M(W')$ (GeV) | $\sigma_{\text{nlo}}^{\text{CT10}}(tW'^- + \bar{t}W'^+) \text{ (pb)}$ | | | $\sigma_{\text{nlo}}^{\text{MSTW 2008 NLO}}(tW'^- + \bar{t}W'^+) \text{ (pb)}$ | | |
|---------------|---|----------------------|----------------------|--|----------------------|----------------------|
| 200 | 76.0 | +4.9 -5.3 | +2.8 -3.2 | 78.1 | +5.3 -5.6 | +0.9 -0.8 |
| 300 | 26.08 | +1.67 -1.89 | +1.13 -1.22 | 26.66 | +1.77 -1.99 | +0.34 -0.33 |
| 400 | 10.66 | +0.69 -0.80 | +0.55 -0.56 | 10.83 | +0.73 -0.84 | +0.16 -0.16 |
| 500 | 4.88 | +0.33 -0.38 | +0.30 -0.29 | 4.92 | +0.34 -0.40 | +0.09 -0.09 |
| 600 | 2.42 | +0.17 -0.20 | +0.17 -0.16 | 2.42 | +0.17 -0.20 | +0.05 -0.05 |
| 700 | 1.270 | +0.091 -0.108 | +0.104 -0.094 | 1.262 | +0.094 -0.110 | +0.031 -0.031 |
| 800 | 0.699 | +0.052 -0.061 | +0.066 -0.058 | 0.689 | +0.053 -0.062 | +0.019 -0.020 |
| 900 | 0.400 | +0.031 -0.036 | +0.043 -0.036 | 0.390 | +0.031 -0.036 | +0.013 -0.013 |
| 1000 | 0.235 | +0.019 -0.022 | +0.028 -0.024 | 0.227 | +0.019 -0.022 | +0.008 -0.008 |
| 1100 | 0.142 | +0.012 -0.014 | +0.019 -0.016 | 0.136 | +0.012 -0.013 | +0.006 -0.005 |
| 1200 | 0.088 | +0.008 -0.009 | +0.013 -0.011 | 0.083 | +0.007 -0.008 | +0.004 -0.004 |
| 1300 | 0.0550 | +0.0049 -0.0056 | +0.0093 -0.0072 | 0.0512 | +0.0047 -0.0054 | +0.0025 -0.0025 |
| 1400 | 0.0351 | +0.0032 -0.0037 | +0.0066 -0.0050 | 0.0322 | +0.0031 -0.0035 | +0.0017 -0.0017 |
| 1500 | 0.0226 | +0.0021 -0.0024 | +0.0047 -0.0035 | 0.0204 | +0.0020 -0.0023 | +0.0012 -0.0012 |
| 1600 | 0.0148 | +0.0014 -0.0016 | +0.0034 -0.0024 | 0.0131 | +0.0013 -0.0015 | +0.0008 -0.0008 |
| 1700 | 0.0097 | +0.0010 -0.0011 | +0.0025 -0.0017 | 0.0085 | +0.0009 -0.0010 | +0.0006 -0.0006 |
| 1800 | 0.0065 | +0.0007 -0.0008 | +0.0018 -0.0012 | 0.0055 | +0.0006 -0.0007 | +0.0004 -0.0004 |
| 1900 | 0.00433 | +0.00047 -0.00051 | +0.00135 -0.00089 | 0.00363 | +0.00041 -0.00044 | +0.00029 -0.00028 |
| 2000 | 0.00292 | +0.00033 -0.00035 | +0.00100 -0.00064 | 0.00239 | +0.00028 -0.00030 | +0.00021 -0.00020 |

Table 28: The sum of the next-to-leading order cross sections for $pp \rightarrow tW'^-$ and $pp \rightarrow \bar{t}W'^+$ at the 8 TeV LHC.

| $M(W'^+) \text{ (GeV)}$ | $\sigma_{\text{nlo}}^{\text{CT10}}(\bar{t}W'^+) \text{ (pb)}$ | | | $\sigma_{\text{nlo}}^{\text{MSTW 2008 NLO}}(\bar{t}W'^+) \text{ (pb)}$ | | |
|-------------------------|---|------------------------|------------------------|--|------------------------|------------------------|
| 200 | 15.8 | +1.0 -1.1 | +1.3 -1.7 | 17.2 | +1.2 -1.3 | +0.5 -0.5 |
| 300 | 4.94 | +0.32 -0.36 | +0.49 -0.61 | 5.38 | +0.36 -0.41 | +0.20 -0.20 |
| 400 | 1.86 | +0.12 -0.14 | +0.22 -0.26 | 2.01 | +0.14 -0.16 | +0.09 -0.09 |
| 500 | 0.78 | +0.05 -0.06 | +0.11 -0.12 | 0.84 | +0.06 -0.07 | +0.04 -0.04 |
| 600 | 0.359 | +0.026 -0.030 | +0.057 -0.063 | 0.383 | +0.029 -0.034 | +0.022 -0.022 |
| 700 | 0.175 | +0.013 -0.015 | +0.032 -0.034 | 0.185 | +0.015 -0.017 | +0.012 -0.012 |
| 800 | 0.090 | +0.007 -0.008 | +0.019 -0.019 | 0.093 | +0.008 -0.009 | +0.007 -0.007 |
| 900 | 0.048 | +0.004 -0.005 | +0.011 -0.011 | 0.049 | +0.004 -0.005 | +0.004 -0.004 |
| 1000 | 0.0260 | +0.0022 -0.0026 | +0.0071 -0.0066 | 0.0261 | +0.0024 -0.0027 | +0.0023 -0.0023 |
| 1100 | 0.0146 | +0.0013 -0.0015 | +0.0045 -0.0040 | 0.0143 | +0.0014 -0.0015 | +0.0014 -0.0014 |
| 1200 | 0.0084 | +0.0008 -0.0009 | +0.0029 -0.0025 | 0.0080 | +0.0008 -0.0009 | +0.0009 -0.0009 |
| 1300 | 0.0049 | +0.0005 -0.0005 | +0.0019 -0.0016 | 0.0045 | +0.0005 -0.0005 | +0.0005 -0.0005 |
| 1400 | 0.00289 | +0.00029 -0.00033 | +0.00128 -0.00101 | 0.00261 | +0.00028 -0.00031 | +0.00034 -0.00034 |
| 1500 | 0.00173 | +0.00018 -0.00020 | +0.00086 -0.00065 | 0.00151 | +0.00017 -0.00018 | +0.00022 -0.00021 |
| 1600 | 0.00105 | +0.00011 -0.00013 | +0.0006 -0.0004 | 0.00088 | +0.00010 -0.00011 | +0.00014 -0.00014 |
| 1700 | 0.00064 | +0.00007 -0.00008 | +0.00040 -0.00028 | 0.00052 | +0.00006 -0.00007 | +0.00009 -0.00009 |
| 1800 | 0.00039 | +0.00005 -0.00005 | +0.00027 -0.00018 | 0.00030 | +0.00004 -0.00004 | +0.00006 -0.00006 |
| 1900 | 0.000243 | +0.000029 -0.000031 | +0.000189 -0.000121 | 0.000180 | +0.000023 -0.000024 | +0.000039 -0.000038 |
| 2000 | 0.000151 | +0.000019 -0.000020 | +0.000132 -0.000080 | 0.000106 | +0.000014 -0.000015 | +0.000026 -0.000025 |

Table 29: Next-to-leading order cross sections for $pp \rightarrow \bar{t}W'^+$ at the 8 TeV LHC.

| $M(W'^-) \text{ (GeV)}$ | $\sigma_{\text{nlo}}^{\text{CT10}}(tW'^-) \text{ (pb)}$ | | | $\sigma_{\text{nlo}}^{\text{MSTW 2008 NLO}}(tW'^-) \text{ (pb)}$ | | |
|-------------------------|---|----------------------|----------------------|--|----------------------|----------------------|
| 200 | 60.1 | +4.0 -4.2 | +2.6 -2.6 | 60.8 | +4.2 -4.4 | +0.8 -0.8 |
| 300 | 21.11 | +1.36 -1.53 | +1.03 -1.01 | 21.25 | +1.42 -1.57 | +0.31 -0.30 |
| 400 | 8.80 | +0.58 -0.66 | +0.49 -0.46 | 8.81 | +0.60 -0.68 | +0.14 -0.14 |
| 500 | 4.09 | +0.27 -0.32 | +0.26 -0.24 | 4.07 | +0.28 -0.33 | +0.07 -0.07 |
| 600 | 2.05 | +0.14 -0.17 | +0.15 -0.14 | 2.03 | +0.15 -0.17 | +0.04 -0.04 |
| 700 | 1.094 | +0.078 -0.092 | +0.091 -0.080 | 1.076 | +0.080 -0.093 | +0.025 -0.025 |
| 800 | 0.609 | +0.045 -0.053 | +0.057 -0.050 | 0.595 | +0.046 -0.053 | +0.016 -0.016 |
| 900 | 0.352 | +0.027 -0.032 | +0.037 -0.032 | 0.341 | +0.027 -0.032 | +0.010 -0.010 |
| 1000 | 0.209 | +0.017 -0.019 | +0.025 -0.021 | 0.201 | +0.017 -0.019 | +0.007 -0.007 |
| 1100 | 0.127 | +0.010 -0.012 | +0.017 -0.014 | 0.121 | +0.010 -0.012 | +0.005 -0.005 |
| 1200 | 0.0793 | +0.0067 -0.0078 | +0.0116 -0.0094 | 0.0746 | +0.0066 -0.0076 | +0.0032 -0.0031 |
| 1300 | 0.0501 | +0.0044 -0.0051 | +0.0081 -0.0065 | 0.0466 | +0.0043 -0.0049 | +0.0022 -0.0021 |
| 1400 | 0.0322 | +0.0029 -0.0033 | +0.0058 -0.0045 | 0.0295 | +0.0028 -0.0032 | +0.0015 -0.0015 |
| 1500 | 0.0209 | +0.0020 -0.0022 | +0.0042 -0.0032 | 0.0189 | +0.0019 -0.0021 | +0.0011 -0.0010 |
| 1600 | 0.0137 | +0.0013 -0.0015 | +0.0030 -0.0022 | 0.0122 | +0.0012 -0.0014 | +0.0007 -0.0007 |
| 1700 | 0.0091 | +0.0009 -0.0010 | +0.0022 -0.0016 | 0.0080 | +0.0008 -0.0009 | +0.0005 -0.0005 |
| 1800 | 0.00608 | +0.00063 -0.00070 | +0.00162 -0.00114 | 0.00523 | +0.00057 -0.00062 | +0.00038 -0.00036 |
| 1900 | 0.00409 | +0.00044 -0.00048 | +0.00120 -0.00082 | 0.00345 | +0.00039 -0.00042 | +0.00027 -0.00026 |
| 2000 | 0.00277 | +0.00031 -0.00033 | +0.00089 -0.00060 | 0.00228 | +0.00026 -0.00028 | +0.00019 -0.00018 |

Table 30: Next-to-leading order cross sections for $pp \rightarrow tW'^-$ at the 8 TeV LHC.

| $M(Z') \text{ (GeV)}$ | $\sigma_{\text{born}}^{\text{CTEQ6L1}}(tZ' + \bar{t}Z') \text{ (pb)}$ | $\sigma_{\text{born}}^{\text{MSTW 2008 LO}}(tZ' + \bar{t}Z') \text{ (pb)}$ |
|-----------------------|---|--|
| 200 | 8.1 +1.3 -1.1 +0.41 | 10.1 +1.7 -1.4 +0.58 |
| 300 | 2.32 -0.33 +0.15 | 3.07 -0.47 +0.23 |
| 400 | 0.81 -0.12 +0.063 | 1.12 -0.18 +0.101 |
| 500 | 0.317 -0.050 +0.028 | 0.461 -0.078 +0.048 |
| 600 | 0.136 -0.022 +0.014 | 0.207 -0.036 +0.024 |
| 700 | 0.063 -0.010 +0.007 | 0.100 -0.018 +0.013 |
| 800 | 0.030 -0.005 +0.0035 | 0.050 -0.009 +0.0069 |
| 900 | 0.0153 -0.0027 +0.0019 | 0.0266 -0.0051 +0.0039 |
| 1000 | 0.0080 -0.0014 +0.0010 | 0.0145 -0.0029 +0.0022 |
| 1100 | 0.0043 -0.0008 +0.0006 | 0.0081 -0.0016 +0.0013 |
| 1200 | 0.0024 -0.0004 +0.00033 | 0.0047 -0.0010 +0.00079 |
| 1300 | 0.00133 -0.00025 +0.00019 | 0.00272 -0.00057 +0.00048 |
| 1400 | 0.00076 -0.00014 +0.00011 | 0.00162 -0.00034 +0.00030 |
| 1500 | 0.00044 -0.00008 +0.00007 | 0.00098 -0.00021 +0.00019 |
| 1600 | 0.00026 -0.00005 +0.000040 | 0.00060 -0.00013 +0.000116 |
| 1700 | 0.000154 -0.000030 +0.000024 | 0.000368 -0.000082 +0.000074 |
| 1800 | 0.000092 -0.000018 +0.000015 | 0.000229 -0.000052 +0.000047 |
| 1900 | 0.000056 -0.000011 +0.000009 | 0.000144 -0.000033 +0.000030 |
| 2000 | 0.000034 -0.000007 | 0.000091 -0.000021 |

Table 31: The sum of the leading order cross sections for $pp \rightarrow tZ'$ and $pp \rightarrow \bar{t}Z'$ at the 8 TeV LHC. Where Z' couples to tc .

| $M(Z')$ (GeV) | $\sigma_{\text{nlo}}^{\text{CT10}}(tZ' + \bar{t}Z')$ (pb) | | | $\sigma_{\text{nlo}}^{\text{MSTW 2008 NLO}}(tZ' + \bar{t}Z')$ (pb) | | |
|---------------|---|------------------------|------------------------|--|------------------------|------------------------|
| 200 | 11.8 | +0.6 -0.6 | +1.3 -1.1 | 12.5 | +0.7 -0.7 | +0.5 -0.7 |
| 300 | 3.50 | +0.18 -0.20 | +0.48 -0.42 | 3.70 | +0.20 -0.22 | +0.19 -0.24 |
| 400 | 1.26 | +0.07 -0.08 | +0.22 -0.19 | 1.33 | +0.07 -0.08 | +0.08 -0.10 |
| 500 | 0.518 | +0.028 -0.033 | +0.107 -0.090 | 0.541 | +0.031 -0.036 | +0.039 -0.047 |
| 600 | 0.232 | +0.013 -0.016 | +0.057 -0.047 | 0.240 | +0.015 -0.017 | +0.020 -0.024 |
| 700 | 0.112 | +0.007 -0.008 | +0.032 -0.025 | 0.114 | +0.007 -0.008 | +0.011 -0.012 |
| 800 | 0.057 | +0.004 -0.004 | +0.019 -0.014 | 0.057 | +0.004 -0.004 | +0.006 -0.007 |
| 900 | 0.0300 | +0.0020 -0.0023 | +0.0113 -0.0083 | 0.0298 | +0.0021 -0.0024 | +0.0034 -0.0039 |
| 1000 | 0.0164 | +0.0011 -0.0013 | +0.0070 -0.0049 | 0.0161 | +0.0012 -0.0013 | +0.0020 -0.0023 |
| 1100 | 0.0093 | +0.0007 -0.0008 | +0.0045 -0.0030 | 0.0089 | +0.0007 -0.0008 | +0.0012 -0.0014 |
| 1200 | 0.0054 | +0.0004 -0.0005 | +0.0029 -0.0019 | 0.0051 | +0.0004 -0.0005 | +0.0008 -0.0008 |
| 1300 | 0.00319 | +0.00024 -0.00028 | +0.00191 -0.00120 | 0.00295 | +0.00024 -0.00027 | +0.00048 -0.00051 |
| 1400 | 0.00192 | +0.00015 -0.00018 | +0.00128 -0.00078 | 0.00174 | +0.00014 -0.00017 | +0.00030 -0.00032 |
| 1500 | 0.00118 | +0.00010 -0.00011 | +0.00087 -0.00051 | 0.00104 | +0.00009 -0.00010 | +0.00019 -0.00020 |
| 1600 | 0.00073 | +0.00006 -0.00007 | +0.00059 -0.00034 | 0.00063 | +0.00006 -0.00006 | +0.00013 -0.00013 |
| 1700 | 0.00046 | +0.00004 -0.00005 | +0.00041 -0.00023 | 0.000384 | +0.00004 -0.00004 | +0.00008 -0.00008 |
| 1800 | 0.000291 | +0.000027 -0.000030 | +0.000287 -0.000152 | 0.000237 | +0.000023 -0.000025 | +0.000053 -0.000054 |
| 1900 | 0.000187 | +0.000018 -0.000020 | +0.000202 -0.000103 | 0.000147 | +0.000015 -0.000016 | +0.000035 -0.000035 |
| 2000 | 0.000120 | +0.000012 -0.000013 | +0.000143 -0.000070 | 0.000092 | +0.000010 -0.000010 | +0.000023 -0.000023 |

Table 32: The sum of the next-to-leading order cross sections for $pp \rightarrow tZ'$ and $pp \rightarrow \bar{t}Z'$ at the 8 TeV LHC. Where Z' couples to tc .

| $M(W')$ (GeV) | $\sigma_{\text{born}}^{\text{CTEQ6L1}}(tW'^- + \bar{t}W'^+) \text{ (pb)}$ | $\sigma_{\text{born}}^{\text{MSTW 2008 LO}}(tW'^- + \bar{t}W'^+) \text{ (pb)}$ |
|---------------|---|--|
| 200 | 13.5 +2.6 -2.0 +0.84 | 15.0 +3.0 -2.3 +0.99 |
| 300 | 4.05 -0.65 +0.32 | 4.58 -0.76 +0.39 |
| 400 | 1.46 -0.25 +0.14 | 1.68 -0.29 +0.13 |
| 500 | 0.59 -0.10 +0.063 | 0.69 -0.13 +0.079 |
| 600 | 0.263 -0.047 +0.031 | 0.313 -0.059 +0.040 |
| 700 | 0.124 -0.023 +0.016 | 0.150 -0.029 +0.021 |
| 800 | 0.062 -0.012 +0.008 | 0.076 -0.015 +0.011 |
| 900 | 0.032 -0.006 +0.0045 | 0.040 -0.008 +0.0062 |
| 1000 | 0.0171 -0.0033 +0.0025 | 0.0218 -0.0045 +0.0036 |
| 1100 | 0.0094 -0.0018 +0.0014 | 0.0122 -0.0026 +0.0021 |
| 1200 | 0.0053 -0.0011 +0.0008 | 0.0070 -0.0015 +0.0013 |
| 1300 | 0.0030 -0.0006 +0.0005 | 0.0041 -0.0009 +0.0008 |
| 1400 | 0.0018 -0.0004 +0.00029 | 0.0024 -0.0005 +0.00046 |
| 1500 | 0.00103 -0.00021 +0.00018 | 0.00145 -0.00033 +0.00029 |
| 1600 | 0.00062 -0.00013 +0.00011 | 0.00088 -0.00020 +0.00018 |
| 1700 | 0.00037 -0.00008 +0.00007 | 0.00054 -0.00013 +0.00011 |
| 1800 | 0.00023 -0.00005 +0.000041 | 0.00034 -0.00008 +0.000072 |
| 1900 | 0.000137 -0.000029 +0.000025 | 0.000211 -0.000050 +0.000046 |
| 2000 | 0.000084 -0.000018 | 0.000133 -0.000032 -0.000026 |

Table 33: The sum of the leading order cross sections for $pp \rightarrow tW'^-$ and $pp \rightarrow \bar{t}W'^+$ and at the 8 TeV LHC. Where W' couples to ts .

| $M(W')$ (GeV) | $\sigma_{\text{nlo}}^{\text{CT10}}(tW'^- + \bar{t}W'^+) \text{ (pb)}$ | | | $\sigma_{\text{nlo}}^{\text{MSTW 2008 NLO}}(tW'^- + \bar{t}W'^+) \text{ (pb)}$ | | |
|---------------|---|------------------------------------|------------------------------------|--|------------------------------------|------------------------------------|
| 200 | 20.3 | +1.3 -1.3 +0.4 | +4.4 -2.5 +1.4 | 21.0 | +1.3 -1.4 +0.4 | +1.2 -1.0 +0.4 |
| 300 | 6.1 | -0.4 +0.14 -0.16 | -0.8 +0.56 -0.35 | 6.4 | -0.4 +0.15 -0.17 | -0.4 +0.17 -0.17 |
| 400 | 2.23 | +0.06 -0.07 +0.028 | +0.25 -0.16 +0.125 | 2.36 | +0.07 -0.08 +0.031 | +0.08 -0.08 +0.040 |
| 500 | 0.92 | -0.033 +0.014 -0.016 | -0.081 +0.066 -0.043 | 0.98 | -0.036 +0.016 -0.018 | -0.040 +0.021 -0.021 |
| 600 | 0.412 | +0.007 -0.009 +0.004 | +0.037 -0.024 +0.021 | 0.213 | +0.008 -0.010 +0.005 | +0.012 -0.012 +0.007 |
| 700 | 0.198 | -0.005 +0.0023 -0.0027 | -0.014 +0.0129 -0.0081 | 0.108 | -0.005 +0.0026 -0.0029 | -0.007 +0.0041 -0.0038 |
| 800 | 0.053 | +0.0013 -0.0015 +0.0008 | +0.0080 -0.0049 +0.0051 | 0.0308 | +0.0015 -0.0017 +0.0009 | +0.0025 -0.0023 +0.0015 |
| 900 | 0.0289 | -0.0009 +0.0005 -0.0006 | -0.0031 +0.0033 -0.0019 | 0.0172 | -0.0010 +0.0005 -0.0006 | -0.0014 +0.0010 -0.0008 |
| 1000 | 0.0163 | +0.00030 -0.00034 +0.00019 | +0.00219 -0.00124 +0.00147 | 0.0098 | +0.00032 -0.00036 +0.00020 | +0.00061 -0.00052 +0.00039 |
| 1100 | 0.0094 | -0.00021 +0.00012 -0.00013 | -0.00081 +0.00100 -0.00053 | 0.0057 | -0.00022 +0.00012 -0.00014 | -0.00033 +0.00026 -0.00021 |
| 1200 | 0.0055 | +0.00008 -0.00009 +0.00005 | +0.00069 -0.00035 +0.00048 | 0.00120 | +0.00008 -0.00009 +0.00005 | +0.00017 -0.00013 +0.00011 |
| 1300 | 0.00329 | -0.00006 +0.000033 -0.000036 | -0.00023 +0.000341 -0.000157 | 0.00073 | -0.00005 +0.000031 -0.000034 | -0.00008 +0.000073 -0.000054 |
| 1400 | 0.00305 | +0.000022 -0.000023 | +0.000242 -0.000107 | 0.00045 | +0.000020 -0.000021 | +0.000049 -0.000035 |
| 1500 | 0.00200 | | | 0.000274 | | |
| 1600 | 0.00123 | | | 0.000170 | | |
| 1700 | 0.00077 | | | | | |
| 1800 | 0.00048 | | | | | |
| 1900 | 0.000305 | | | | | |
| 2000 | 0.000195 | | | | | |

Table 34: The sum of the next-to-leading order cross sections for $pp \rightarrow tW'^-$ and $pp \rightarrow \bar{t}W'^+$ at the 8 TeV LHC. Where W' couples to ts .

| $M(W')$ (GeV) | $\sigma_{\text{born}}^{\text{CTEQ6L1}}(tW'^- + \bar{t}W'^+) \text{ (pb)}$ | $\sigma_{\text{born}}^{\text{MSTW 2008 LO}}(tW'^- + \bar{t}W'^+) \text{ (pb)}$ |
|---------------|---|--|
| 200 | 4.94 +0.57 -0.54 +0.17 | 6.10 +0.76 -0.68 +0.24 |
| 300 | 1.42 -0.16 +0.066 | 1.83 -0.22 +0.101 |
| 400 | 0.491 -0.059 +0.028 | 0.658 -0.087 +0.045 |
| 500 | 0.193 -0.025 +0.013 | 0.268 -0.038 +0.022 |
| 600 | 0.083 -0.011 +0.006 | 0.119 -0.018 +0.011 |
| 700 | 0.0378 -0.005 +0.0032 | 0.056 -0.009 +0.0058 |
| 800 | 0.0182 -0.0026 +0.0017 | 0.0282 -0.0046 +0.0032 |
| 900 | 0.0092 -0.0014 +0.0009 | 0.0147 -0.0025 +0.0018 |
| 1000 | 0.0048 -0.0007 +0.0005 | 0.0079 -0.0014 +0.0010 |
| 1100 | 0.0026 -0.0004 +0.00028 | 0.0044 -0.0008 +0.00060 |
| 1200 | 0.00141 -0.00022 +0.00016 | 0.00248 -0.00046 +0.00036 |
| 1300 | 0.00079 -0.00013 +0.00009 | 0.00143 -0.00027 +0.00022 |
| 1400 | 0.00045 -0.00007 +0.00006 | 0.00084 -0.00016 +0.00013 |
| 1500 | 0.00026 -0.00004 +0.000033 | 0.00050 -0.00010 +0.000082 |
| 1600 | 0.000154 -0.000026 +0.000020 | 0.000302 -0.000061 +0.000052 |
| 1700 | 0.000091 -0.000016 +0.000012 | 0.000184 -0.000038 +0.000032 |
| 1800 | 0.000055 -0.000010 +0.000007 | 0.000113 -0.000024 +0.000021 |
| 1900 | 0.000033 -0.000006 +0.000005 | 0.000070 -0.000015 +0.000013 |
| 2000 | 0.000020 -0.000004 | 0.000044 -0.000010 |

Table 35: The sum of the leading order cross sections for $pp \rightarrow tW'^-$ and $pp \rightarrow \bar{t}W'^+$ at the 8 TeV LHC. Where W' couples to tb .

| $M(W')$ (GeV) | $\sigma_{\text{nlo}}^{\text{CT10}}(tW'^- + \bar{t}W'^+) \text{ (pb)}$ | | | $\sigma_{\text{nlo}}^{\text{MSTW 2008 NLO}}(tW'^- + \bar{t}W'^+) \text{ (pb)}$ | | |
|---------------|---|-----------|-----------|--|-----------|-----------|
| 200 | 6.93 | +0.45 | +0.74 | 7.50 | +0.48 | +0.30 |
| | | -0.40 | -0.65 | | -0.42 | -0.39 |
| 300 | 2.04 | +0.12 | +0.28 | 2.20 | +0.13 | +0.11 |
| | | -0.10 | -0.24 | | -0.10 | -0.14 |
| 400 | 0.736 | +0.040 | +0.125 | 0.787 | +0.043 | +0.047 |
| | | -0.031 | -0.106 | | -0.034 | -0.057 |
| 500 | 0.301 | +0.016 | +0.061 | 0.319 | +0.017 | +0.022 |
| | | -0.013 | -0.051 | | -0.015 | -0.026 |
| 600 | 0.134 | +0.007 | +0.032 | 0.141 | +0.007 | +0.011 |
| | | -0.006 | -0.026 | | -0.007 | -0.013 |
| 700 | 0.0643 | +0.0030 | +0.0179 | 0.0667 | +0.0031 | +0.0059 |
| | | -0.0032 | -0.0139 | | -0.0036 | -0.0068 |
| 800 | 0.0325 | +0.0015 | +0.0104 | 0.0333 | +0.0016 | +0.0033 |
| | | -0.0017 | -0.0078 | | -0.0019 | -0.0037 |
| 900 | 0.0171 | +0.0008 | +0.0063 | 0.0173 | +0.0009 | +0.0019 |
| | | -0.0010 | -0.0045 | | -0.0011 | -0.0021 |
| 1000 | 0.0093 | +0.0005 | +0.0039 | 0.0093 | +0.0005 | +0.0011 |
| | | -0.0006 | -0.0027 | | -0.0006 | -0.0012 |
| 1100 | 0.00525 | +0.00027 | +0.00244 | 0.00513 | +0.00029 | +0.00067 |
| | | -0.00033 | -0.00162 | | -0.00035 | -0.00072 |
| 1200 | 0.00303 | +0.00017 | +0.00157 | 0.00290 | +0.00017 | +0.00041 |
| | | -0.00020 | -0.00100 | | -0.00021 | -0.00043 |
| 1300 | 0.00178 | +0.00010 | +0.00103 | 0.00167 | +0.00010 | +0.00025 |
| | | -0.00012 | -0.00063 | | -0.00012 | -0.00027 |
| 1400 | 0.00107 | +0.00006 | +0.00069 | 0.00098 | +0.00006 | +0.00016 |
| | | -0.00008 | -0.00041 | | -0.00008 | -0.00017 |
| 1500 | 0.00065 | +0.00004 | +0.00046 | 0.00058 | +0.00004 | +0.00010 |
| | | -0.00005 | -0.00027 | | -0.00005 | -0.00011 |
| 1600 | 0.000400 | +0.000026 | +0.000315 | 0.000351 | +0.000025 | +0.000065 |
| | | -0.000032 | -0.000174 | | -0.000029 | -0.000066 |
| 1700 | 0.000250 | +0.000017 | +0.000216 | 0.000213 | +0.000016 | +0.000042 |
| | | -0.000021 | -0.000116 | | -0.000018 | -0.000042 |
| 1800 | 0.000157 | +0.000011 | +0.000150 | 0.000131 | +0.000010 | +0.000027 |
| | | -0.000013 | -0.000078 | | -0.000012 | -0.000027 |
| 1900 | 0.000100 | +0.000007 | +0.000105 | 0.000081 | +0.000006 | +0.000018 |
| | | -0.000009 | -0.000052 | | -0.000008 | -0.000018 |
| 2000 | 0.000064 | +0.000005 | +0.000074 | 0.000050 | +0.000004 | +0.000012 |
| | | -0.000006 | -0.000036 | | -0.000005 | -0.000012 |

Table 36: The sum of the next-to-Leading order cross sections for $pp \rightarrow tW'^-$ and $pp \rightarrow \bar{t}W'^+$ at the 8 TeV LHC. Where W' couples to tb .

References

- [1] J. H. Kühn and G. Rodrigo, “Charge asymmetry in hadroproduction of heavy quarks,” *Phys. Rev. Lett.* **81** (1998) 49–52.
- [2] L. G. Almeida, G. Sterman, and W. Vogelsang, “Threshold resummation for the top quark charge asymmetry,” *Phys. Rev. D* **78** (2008) 014008.
- [3] N. Kidonakis, “Top quark rapidity distribution and forward-backward asymmetry,” *Phys. Rev. D* **84** (2011) 011504.
- [4] V. Ahrens, A. Ferroglia, M. Neubert, B. D. Pecjak and L. L. Yang, “The top-pair forward-backward asymmetry beyond NLO,” *Phys. Rev. D* **84** (2011) 074004.
- [5] W. Hollik and D. Pagani, “Electroweak contribution to the top quark forward-backward asymmetry at the tevatron,” *Phys. Rev. D* **84** (2011) 093003.
- [6] A. V. Manohar and M. Trott, “Electroweak sudakov corrections and the top quark forward-backward asymmetry,” *Phys.Lett. B* **711** (2012) 313–316.
- [7] F. Halzen, P. Hoyer, and C. Kim, “Forward-Backward asymmetry of hadroproduced heavy quarks in QCD,” *Phys.Lett.* **B195** (1987) 74.
- [8] **CDF** Collaboration, T. Aaltonen *et al.*, “Evidence for a Mass Dependent Forward-Backward Asymmetry in Top Quark Pair Production,” *Phys.Rev.* **D83** (2011) 112003.
- [9] **D0** Collaboration, V. M. Abazov *et al.*, “Forward-backward asymmetry in top quark-antiquark production,” *Phys.Rev.* **D84** (2011) 112005.
- [10] **D0** Collaboration, V. Abazov *et al.*, “First measurement of the forward-backward charge asymmetry in top quark pair production,” *Phys.Rev.Lett.* **100** (2008) 142002.
- [11] K. Cheung, W.-Y. Keung, and T.-C. Yuan, “Top Quark Forward-Backward Asymmetry,” *Phys.Lett.* **B682** (2009) 287–290.
- [12] K. Cheung and T.-C. Yuan, “Top Quark Forward-Backward Asymmetry in the Large Invariant Mass Region,” *Phys.Rev.* **D83** (2011) 074006.
- [13] B. Bhattacharjee, S. S. Biswal, and D. Ghosh, “Top quark forward-backward asymmetry at Tevatron and its implications at the LHC,” *Phys.Rev.* **D83** (2011) 091501.
- [14] V. Barger, W.-Y. Keung, and C.-T. Yu, “Tevatron Asymmetry of Tops in a W', Z' Model,” *Phys.Lett.* **B698** (2011) 243–250.
- [15] N. Craig, C. Kilic, and M. J. Strassler, “LHC Charge Asymmetry as Constraint on Models for the Tevatron Top Anomaly,” *Phys.Rev.* **D84** (2011) 035012.
- [16] C.-H. Chen, S. S. Law, and R.-H. Li, “Rare B decays and Tevatron top-pair asymmetry,” *J.Phys.G* **G38** (2011) 115008.
- [17] K. Yan, J. Wang, D. Y. Shao, and C. S. Li, “Next-to-leading order QCD effect of W' on top quark Forward-Backward Asymmetry,” *Phys.Rev.* **D85** (2012) 034020.

- [18] S. Knapen, Y. Zhao, and M. J. Strassler, “Diagnosing the Top-Quark Angular Asymmetry using LHC Intrinsic charge Asymmetries,” *Phys.Rev.* **D86** (2012) 014013.
- [19] S. Jung, H. Murayama, A. Pierce, and J. D. Wells, “Top quark forward-backward asymmetry from new t-channel physics,” *Phys.Rev.* **D81** (2010) 015004.
- [20] B. Xiao, Y.-k. Wang, and S.-h. Zhu, “Forward-backward Asymmetry and Differential Cross Section of Top Quark in Flavor Violating Z’ model at $\mathcal{O}(\alpha_s^2\alpha_X)$,” *Phys.Rev.* **D82** (2010) 034026.
- [21] J. Cao, L. Wang, L. Wu, and J. M. Yang, “Top quark forward-backward asymmetry, FCNC decays and like-sign pair production as a joint probe of new physics,” *Phys.Rev.* **D84** (2011) 074001.
- [22] E. L. Berger, Q.-H. Cao, C.-R. Chen, C. S. Li, and H. Zhang, “Top Quark Forward-Backward Asymmetry and Same-Sign Top Quark Pairs,” *Phys.Rev.Lett.* **106** (2011) 201801.
- [23] J. Aguilar-Saavedra and M. Perez-Victoria, “No like-sign tops at Tevatron: Constraints on extended models and implications for the t tbar asymmetry,” *Phys.Lett.* **B701** (2011) 93–100.
- [24] D.-W. Jung, P. Ko, and J. S. Lee, “Possible Common Origin of the Top Forward-backward Asymmetry and the CDF Dijet Resonance,” *Phys.Rev.* **D84** (2011) 055027.
- [25] M. Duraissamy, A. Rashed, and A. Datta, “The Top Forward Backward Asymmetry with general Z’ couplings,” *Phys.Rev.* **D84** (2011) 054018.
- [26] P. Ko, Y. Omura, and C. Yu, “Top Forward-Backward Asymmetry in Chiral U(1)’ Models,” *Nuovo Cim.* **C035N3** (2012) 245–248.
- [27] P. Ko, Y. Omura, and C. Yu, “Top Forward-Backward Asymmetry and the CDF Wjj Excess in Leptophobic $U(1)'$ Flavor Models,” *Phys.Rev.* **D85** (2012) 115010.
- [28] E. L. Berger, “Tevatron Top Quark Forward-Backward Asymmetry – Implications for Same-sign Top Quark Pair Production,” [arXiv:1109.3202](https://arxiv.org/abs/1109.3202).
- [29] M. I. Gresham, I.-W. Kim, and K. M. Zurek, “Searching for Top Flavor Violating Resonances,” *Phys.Rev.* **D84** (2011) 034025.
- [30] D. Duffy, Z. Sullivan, and H. Zhang, “Top quark forward-backward asymmetry and W’ bosons,” *Phys.Rev.* **D85** (2012) 094027.
- [31] S. Y. Ayazi, S. Khatibi, and M. M. Najafabadi, “Top Quark Forward-Backward Asymmetry and W' -Boson with General Couplings,” *JHEP* **1210** (2012) 103.
- [32] Y. Zhang, S.-Z. Jiang, and Q. Wang, “The Global Electroweak Fit and its Implication to Z-prime,” [arXiv:1205.3567](https://arxiv.org/abs/1205.3567).
- [33] J. Aguilar-Saavedra and M. Perez-Victoria, “Simple models for the top asymmetry: Constraints and predictions,” *JHEP* **1109** (2011) 097.
- [34] S. Jung, A. Pierce, and J. D. Wells, “Top asymmetry and the search for a light hadronic resonance in association with single top,” *Phys.Rev.* **D84** (2011) 091502.

- [35] E. L. Berger, Q.-H. Cao, J.-H. Yu, and C.-P. Yuan, “Calculation of Associated Production of a Top Quark and a W' at the LHC,” *Phys.Rev.* **D84** (2011) 095026.
- [36] J. Cao, K. Hikasa, L. Wang, L. Wu, and J. M. Yang, “Testing new physics models by top charge asymmetry and polarization at the LHC,” *Phys.Rev.* **D85** (2012) 014025.
- [37] T. Jezo, M. Klasen, and I. Schienbein, “LHC phenomenology of general $SU(2)_C \times SU(2)_L \times U(1)_Y$ models,” *Phys.Rev.* **D86** (2012) 035005.
- [38] Q.-H. Cao, Z. Li, J.-H. Yu, and C. Yuan, “Discovery and Identification of W' and Z' in $SU(2)_C \times SU(2)_L \times U(1)_Y$ Models at the LHC,” [arXiv:1205.3769](#).
- [39] **ALEPH, CDF, D0, DELPHI, L3, OPAL, SLD Collaborations, the LEP Electroweak Working Group, the Tevatron Electroweak Working Group, and the SLD electroweak and heavy flavour groups** Collaboration, “Precision electroweak measurements and constraints on the Standard Model,” FERMILAB-TM-2480-PPD, CERN-PH-EP-2010-095, SLAC-PUB-14301.
- [40] I. Altarev, Y. Borisov, N. Borovikova, S. Ivanov, E. Kolomensky, *et al.*, “New measurement of the electric dipole moment of the neutron,” *Phys.Lett.* **B276** (1992) 242–246.
- [41] I. Altarev, Y. Borisov, N. Borovikova, A. Egorov, S. Ivanov, *et al.*, “Search for the neutron electric dipole moment,” *Phys.Atom.Nucl.* **59** (1996) 1152–1170.
- [42] **CMS** Collaboration, S. Chatrchyan *et al.*, “Search for Same-Sign Top-Quark Pair Production at $\sqrt{s} = 7$ TeV and Limits on Flavour Changing Neutral Currents in the Top Sector,” *JHEP* **1108** (2011) 005.
- [43] **ATLAS** Collaboration, G. Aad *et al.*, “Search for same-sign top-quark production and fourth-generation down-type quarks in pp collisions at $\sqrt{s} = 7$ TeV with the ATLAS detector,” *JHEP* **1204** (2012) 069.
- [44] **D0** Collaboration, V. M. Abazov *et al.*, “Measurement of the $t\bar{t}$ production cross section using dilepton events in $p\bar{p}$ collisions,” *Phys.Lett.* **B704** (2011) 403–410.
- [45] **CDF** Collaboration, T. Aaltonen *et al.*, “Measurement of the Top Pair Production Cross Section in the Lepton + Jets Channel Using a Jet Flavor Discriminant,” *Phys.Rev.* **D84** (2011) 031101.
- [46] **CMS** Collaboration, S. Chatrchyan *et al.*, “Measurement of the top quark pair production cross section in pp collisions at $\sqrt{s} = 7$ TeV in dilepton final states containing a tau,” [arXiv:1203.6810](#).
- [47] **ATLAS** Collaboration, G. Aad *et al.*, “Measurement of the top quark pair cross section with ATLAS in pp collisions at $\sqrt{s} = 7$ TeV using final states with an electron or a muon and a hadronically decaying tau lepton,” *Phys.Lett.* **B717** (2012) 89–108.
- [48] **CMS Collaboration** Collaboration, S. Chatrchyan *et al.*, “Measurement of the charge asymmetry in top-quark pair production in proton-proton collisions at $\sqrt{s} = 7$ TeV,” *Phys.Lett.* **B709** (2012) 28–49.

- [49] **ATLAS Collaboration** Collaboration, G. Aad *et al.*, “Measurement of the charge asymmetry in top quark pair production in pp collisions at $\sqrt{s} = 7$ TeV using the ATLAS detector,” *Eur.Phys.J.* **C72** (2012) 2039.
- [50] J. Chakraborty, J. Gluza, R. Sevillano, and R. Szafron, “Left-right symmetry at LHC and precise 1-loop low energy data,” *JHEP* **1207** (2012) 038.
- [51] **CDF Collaboration**, T. Aaltonen *et al.*, “Search for a heavy particle decaying to a top quark and a light quark in $p\bar{p}$ collisions at $\sqrt{s} = 1.96$ TeV,” *Phys.Rev.Lett.* **108** (2012) 211805.
- [52] **CMS Collaboration**, S. Chatrchyan *et al.*, “Search for charge-asymmetric production of W bosons in top pair + jet events from pp collisions at $\sqrt{s} = 7$ TeV,” [arXiv:1206.3921](#).
- [53] T. M. Tait, “The tW^- mode of single top production,” *Phys.Rev.* **D61** (2000) 034001.
- [54] J. M. Campbell and F. Tramontano, “Next-to-leading order corrections to Wt production and decay,” *Nucl.Phys.* **B726** (2005) 109–130.
- [55] S. Zhu, “Next-to-leading order QCD corrections to $bg \rightarrow tW^-$ at the CERN Large Hadron Collider,” *Phys.Lett.* **B524** (2002) 283–288.
- [56] S. Frixione, E. Laenen, P. Motylinski, B. R. Webber, and C. D. White, “Single-top hadroproduction in association with a W boson,” *JHEP* **0807** (2008) 029.
- [57] C. Weydert, S. Frixione, M. Herquet, M. Klasen, E. Laenen, *et al.*, “Charged Higgs boson production in association with a top quark in MC@NLO,” *Eur.Phys.J.* **C67** (2010) 617–636.
- [58] J. C. Collins, F. Wilczek, and A. Zee, “Low-Energy Manifestations of Heavy Particles: Application to the Neutral Current,” *Phys.Rev.* **D18** (1978) 242.
- [59] R. K. Ellis and G. Zanderighi, “Scalar one-loop integrals for QCD,” *JHEP* **0802** (2008) 002.
- [60] A. Belyaev, E. Boos, and L. Dudko, “Single top quark at future hadron colliders: Complete signal and background study,” *Phys.Rev.* **D59** (1999) 075001.
- [61] N. Kauer and D. Zeppenfeld, “Finite width effects in top quark production at hadron colliders,” *Phys.Rev.* **D65** (2002) 014021.
- [62] B. P. Kersevan and I. Hinchliffe, “A Consistent prescription for the production involving massive quarks in hadron collisions,” *JHEP* **0609** (2006) 033.
- [63] C. D. White, S. Frixione, E. Laenen, and F. Maltoni, “Isolating Wt production at the LHC,” *JHEP* **0911** (2009) 074.
- [64] E. Re, “Single-top Wt -channel production matched with parton showers using the POWHEG method,” *Eur.Phys.J.* **C71** (2011) 1547.
- [65] S. Frixione, Z. Kunszt, and A. Signer, “Three jet cross-sections to next-to-leading order,” *Nucl.Phys.* **B467** (1996) 399–442.
- [66] S. Frixione, “Colourful FKS subtraction,” *JHEP* **1109** (2011) 091.

- [67] S. Catani and M. Seymour, “The Dipole formalism for the calculation of QCD jet cross-sections at next-to-leading order,” *Phys.Lett.* **B378** (1996) 287–301.
- [68] S. Catani and M. Seymour, “A General algorithm for calculating jet cross-sections in NLO QCD,” *Nucl.Phys.* **B485** (1997) 291–419.
- [69] C. Chung, M. Kramer, and T. Robens, “An alternative subtraction scheme for next-to-leading order QCD calculations,” *JHEP* **1106** (2011) 144.
- [70] J. Pumplin, D. Stump, J. Huston, H. Lai, P. M. Nadolsky, *et al.*, “New generation of parton distributions with uncertainties from global QCD analysis,” *JHEP* **0207** (2002) 012.
- [71] H.-L. Lai, M. Guzzi, J. Huston, Z. Li, P. M. Nadolsky, *et al.*, “New parton distributions for collider physics,” *Phys.Rev.* **D82** (2010) 074024.
- [72] A. Martin, W. Stirling, R. Thorne, and G. Watt, “Parton distributions for the LHC,” *Eur.Phys.J.* **C63** (2009) 189–285.
- [73] M. Botje, J. Butterworth, A. Cooper-Sarkar, A. de Roeck, J. Feltesse, *et al.*, “The PDF4LHC Working Group Interim Recommendations,” [arXiv:1101.0538](#).
- [74] **ATLAS** Collaboration, G. Aad *et al.*, “Search for top-jet resonances in the lepton+jets channel if $t\bar{t}$ + jets events with the ATLAS detector in 4.7 fb^{-1} of pp collisions at $\sqrt{s}=7$ TeV,” *ATLAS-CONF-2012-096* (2012).
- [75] **ATLAS Collaboration** Collaboration, G. Aad *et al.*, “Search for resonant top plus jet production in $t\bar{t}$ + jets events with the ATLAS detector in pp collisions at $\sqrt{s}=7$ TeV,” [arXiv:1209.6593](#).
- [76] J. Alwall, M. Herquet, F. Maltoni, O. Mattelaer, and T. Stelzer, “MadGraph 5 : Going Beyond,” *JHEP* **1106** (2011) 128.
- [77] K. Arnold, L. d’Errico, S. Gieseke, D. Grellscheid, K. Hamilton, *et al.*, “Herwig++ 2.6 Release Note,” [arXiv:1205.4902](#).
- [78] M. Endo and S. Iwamoto, “Comment on the CMS search for charge-asymmetric production of W boson in $t\bar{t}$ + jet events,” [arXiv:1207.5900](#).
- [79] F. Olness, J. Pumplin, D. Stump, J. Huston, P. M. Nadolsky, *et al.*, “Neutrino dimuon production and the strangeness asymmetry of the nucleon,” *Eur.Phys.J.* **C40** (2005) 145–156.
- [80] H. Lai, P. M. Nadolsky, J. Pumplin, D. Stump, W. Tung, *et al.*, “The Strange parton distribution of the nucleon: Global analysis and applications,” *JHEP* **0704** (2007) 089.
- [81] W. Tung, H. Lai, A. Belyaev, J. Pumplin, D. Stump, *et al.*, “Heavy Quark Mass Effects in Deep Inelastic Scattering and Global QCD Analysis,” *JHEP* **0702** (2007) 053.